Ho Chi Minh City Semiconductor Industrial Development Program 2017-2020, MEMS Development Program 2017-2020

The 3rd International Workshop on MEMS and Sensor System

IWMS 2019

MEMS and Nanomaterials

August 27-28, 2019

Ho Chi Minh City, Vietnam

Hosted by:

SHTP SAIGON HI-TECH PARK

ĐẠI HỌC QUỐC GIA TP. HỒ CHÍ MINH

KHOA HỌC VÀ CÔNG NGHỆ

ICT

Implementers:

SHTPLABS SAIGON HI-TECH PARK R&D CENTER

INOMAR

NIMS

semi

Table of Contents

WELCOME ADDRESS

Delivered by Le Bich Loan
Chairman of IWMS 2019
Acting President of Saigon High Tech Park

Welcome to the 3rd International Workshop on MEMS and Sensor System 2019 (IWMS 2019) in Ho Chi Minh City, Vietnam. The International Workshop on MEMS and Sensor System originated in 2017, which had been known as the First International Conference on MEMS and Sensor system was held in Ho Chi Minh City, Vietnam. Over the last decade, the MEMS community has experienced immense growth in the science and technology of miniaturization, as well as commercialization. The IWMS events come at a time when MEMS technology has evolved into a key enabler for smart products and the Internet of Things (IoT).

With the advent of globalization and rapid technological advances in the 21st Century, we facing increasing demands to able to effectively harness and exploit these challenges for economic growth. Recognizing the massive growth potential of MicroElectroMechanical Systems (MEMS) and sensors in the IoT applications based on several advanced properties such as low power consumption, low cost, and fast responsibility, and MEMS devices are considered to play an important role for building a smart city.

After the successes of IWMS2017 and IWMS2018, The Research Laboratories of Saigon High Tech Park (SHTPLABS), Center for Innovative Materials and Architectures (INOMAR), Center for Functional Sensor and Actuator (NIMS, Japan), and Semi organize The Third International Workshop on MEMS and Sensor System: Sensor and Materials (IWMS 2019) in order to highlight the latest advances in sensor technology and materials research with a strong emphasis on the interdisciplinary character of these topics.

The sensor session will cover the MEMS, nanomechanical sensor, and biosensor research, etc. The materials session will display a wide range of subtopics, from material chemistry and physics, surface science, interface science, nanoarchitectonics, etc.

Saigon Hi-Tech Park (SHTP) is a science and technology zone in the heart of the most dynamic area of Vietnam - Ho Chi Minh City. From the beginning, we have focused on high tech manufacturing such as semiconductor, biotechnology, and nanotechnology. With several advantage policies and strong support from Ho Chi Minh City government as well as from scientists, we hope that you will find SHTP to be your future home for business.

To organize this workshop, we have received strong support from Ho Chi Committee under the Semiconductor Industrial Development Program in the period of 2017-2020, with a vision toward 2030. We wish to give our acknowledgment to Center for Innovative Materials and Architectures (INOMAR), Center for Functional Sensor and Actuator (NIMS, Japan), and Semi as co-organizers.

We are looking forward to an exciting and high-level scientific and strategic program that will give the opportunity to all delegates for networking and sharing ideas and achievements while enjoying the wonderful experience in Ho Chi Minh city.

Thank you!

A MICROMACHINED IONIC LIQUID ION SOURCE ARRAY

Hiroki Kuwano[1,*], Ryo Yoshida[1], Ngyen Van Chinh[1], Le Van Minh[1]
[1]Tohoku University
*Email: hiroki.kuwano@nanosys.mech.tohoku.ac.jp

This paper describes concurrent reactive ion etching (RIE) using micro ionic liquid ion source (ILIS) array. The ILIS array was successfully fabricated using bulk micromachining and consists of micro needle emitters and a reservoir for the ionic liquid (IL) of 1-ethyl-3-methylimidazolium tetrafluoroborate ([EMIM]-[BF_4]). The ion beam etching of a (100) silicon substrate using the fabricated ILIS array was demonstrated with an ion-accelerated voltage of 5.1 kV. As a result, the etching rate of silicon was 5.6×10^{-4} [μm^3/pA・sec] and was 1.5 times larger than conventional focused Ga^+ ion beam etching.

Key words: focused ion beam, ion liquid, RIE

INTRODUCTION

The multi focused ion beam system as shown in Figure 1 was proposed to apply the focused ion beam (FIB) system to the high-mix low-volume production with high throughput [1]. In this system, the IL was adopted as the source material of ions instead of the conventional liquid metals such as Ga or In. The IL is molten salt that is liquid over a wide temperature range including room temperature. By using the IL, the FIB system can be simplified and miniaturized since the heating unit can be removed. We fabricated the micromachined ILIS array and succeeded in the first detection of reactive ions from the ILIS array [1].

RESULTS

Figure 2 shows scanning electron microscopic (SEM) images of the fabricated ILIS arrays. I-V characteristics was measured and compared of the I-V characteristics between the emitter of ϕ60 μm and thick emitter of ϕ200 μm. It was confirmed that, by increasing the diameter of the emitter, emission current can be increased. Surface tension of liquid plays important role to supply the IL to the emitter tip. When dipping a rod into liquid, the liquid climbs up on the rod surface due to the surface tension. By increasing the diameter of emitter, amount of IL climbing up to the tip can be increased [2].

Figure 3 shows etching marks on (100) silicon substrate using the ILIS array with the diameter of 200 μm and distance of 800 μm. As shown in Figure 3, cone shaped patterns were observed. Etching rate of one ILIS was calculated from the etched volume and was 5.6×10^{-4} [μm^3/pA・sec]. This is 1.5 times higher than etching rate with a conventional focused Ga^+ ion beam [3][4].

Acknowledgement: This work was supported by Grants-in-aid for Scientific Research [A] from MEXT (Grant. No. 16H02093)

References

[1] T. Suzuki, M. Hara, H. Oguchi, and H. Kuwano, *Proc. MEMS 2013*, pp. 315-318.
[2] P. Gennes, F. Brochard-Wyart, and D. Quéré, "Capillarity and wetting phenomena drops, bubbles, pearls, waves", Springer, 2003
[3] M. Lachab, M. Nozaki, J. Wang, Y. Ishikawa, Q. Fareed, T. Wang, T. Nishikawa, K. Nishino, and S. Sakai, *J Appl. Phys.*, 87, pp.1374-1378 (2000)
[4] Ryo Yoshida, Motoaki Hara, Hiroyuki Oguchi, Hiroki Kuwano, *Proc. MEMS 2015*, pp. 93-96.

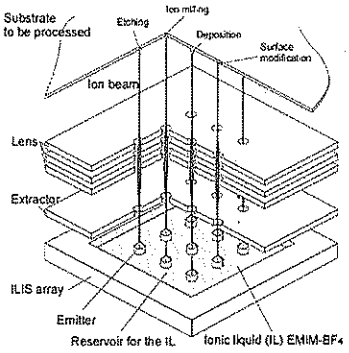

Figure 1: Schematic illustration of the multi-process system based on the focused ion beam

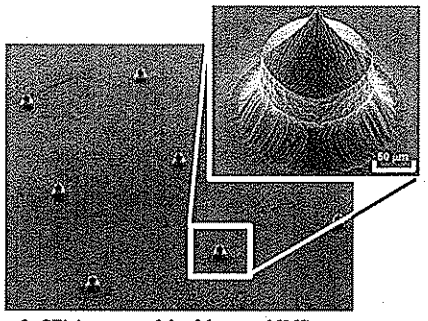

Figure2: SEM images of the fabricated ILIS array.

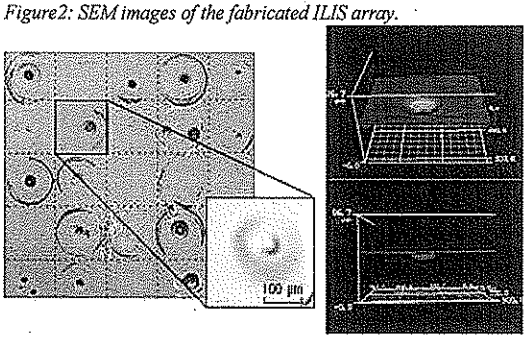

Figure3: Photos (left) and 3D images (right) of patterns on Si etched by emitted multi-ion beams

STRECHABLE WAVY INTERCONNECT AND SENSOR FABRICATGED BY MICRO-CORRUGATION PROCESS

Toshihiro Itoh*, Michitaka Yamamoto, Shinji Okuda, Seiichi Takamatsu
Graduate School of Frontier Sciences, The University of Tokyo
*Email: toshihiro-itoh@edu.k.u-tokyo.ac.jp

We developed a micro-corrugation process to fabricate vertically wavy interconnects and piezoelectric sensor for highly stretchable human motion e-textile devices. Wavy structure is formed by micro-corrugation process where foils and thin films are bent with gears. The fabricated wavy Cu interconnects showed stretchability of more than 40%. Using the 0.5-mm-wide interconnects, FPC (flexible printed circuit)-compatible stretchable electric circuit integrated with LEDs was successfully demonstrated. The fabricated sensor sustains 15% strain and successfully detects the bending motion of the human finger.

Key words: Stretchable Interconnect, Stretchable Sensor, Vertically Wavy Structure, Micro-corrugation Process, PVDF Film

Electronic textiles (e-textiles) are fabrics that are integrated with electronic elements including sensors, actuators and microcontrollers, and are expected to be applied to not only wearables but also smart sheets, for instance. Stretchability is frequently required for e-textiles. For instance, since human skin around the elbow or knee joints can be stretched to more than 30%, interconnects of wearable devices need stretchability of 30% or above. Although stretchable interconnects on textile substrates are often realized by printing horseshoe-patterns with use of "stretchable" inks, printing patterns cannot cover stretch as large as 30% and require large surface areas. To realize fine interconnects with stretchability of 30% or above, we have developed vertical wavy Cu stretchable interconnects utilizing micro-corrugation process of Cu foils and embedding in silicon rubber (Fig. 1). When Cu foils are shriveled to -30% by micro-corrugation, the interconnects should be stretched to 30% without electric resistance change. The micro-corrugation process is based on the metal foil forming technique where a flat Cu foil is continuously deformed into wavy shape of interconnects between the upper and lower gears. After the process, the wavy machined Cu foils are embedded in silicone rubber to protect them and improve the interconnects' elasticity. The fabricated wavy Cu interconnects showed stretchability of more than 40%. Using the 0.5-mm-wide interconnects, FPC(flexible printed circuit)-compatible stretchable electric circuit integrated with LEDs was successfully demonstrated. In addition, we have applied the micro-corrugation process to fabricate a vertically wavy thin film piezoelectric sensor for highly stretchable human motion sensors (Fig. 2). A continuous wavy structured polyvinylidene difluoride film with 600-μm pitch and 140-μm height was successfully fabricated. The fabricated sensor sustains 15% strain and successfully detects the bending motion of the human finger.

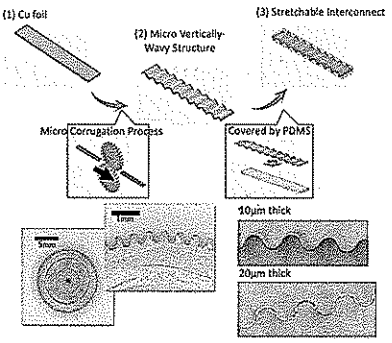

Figure 1: Fabrication process of stretchable Cu interconnects utilizing micro-corrugation.

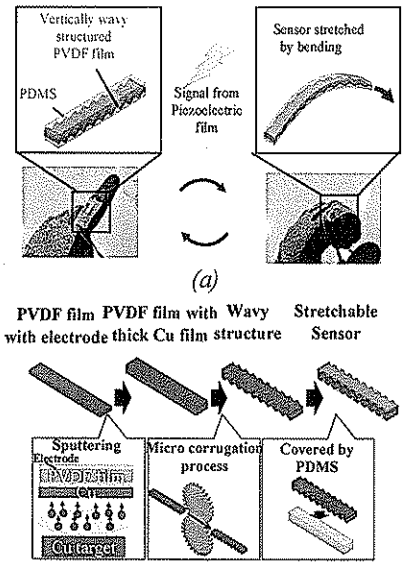

Figure 2 (a) Stretchable wavy piezoelectric sensor, and (b) its fabrication process

CAN WE LEVER A MEMS ALLIANCE IN VIETNAM?

Anh-Tuan Mai
Microfabrication Laboratory at Hoa Lac Hightech Park
National Center for Technological Progress, C6 Thanh Xuan Bac, Thanh Xuan, Hanoi
*Email: matuan@most.gov.vn

Fragmented infrastructure, expensive license for design platform, loosen connection with the industry, lack of manpower. Can we lever a MEMS alliance in Vietnam? An idea to create an alliance in MEMS will be discussed in this work by, first of all, an active and strong network between SHTP and HHTP with the support from experienced experts and global companies.

Key words: MEMS alliance; SHTP; HHTP

SELF-POWERED HYBRID INTEGRATED FLEXIBLE ELECTRONICS MICRO/NANO-SYSTEMS (HIFES)

Chengkuo LEE[1,2,3,4,*], Minglu Zhu[1,2,3,4], Qiongfeng Shi[1,2,3], and Tianyiyi He[1,2,3,4]

[1] Department of Electrical & Computer Engineering, National University of Singapore, 4 Engineering Drive 3, 117576, Singapore
[2] Hybrid Integrated Flexible Electronic Systems (HIFES), 5 Engineering Drive 1, 117608, Singapore
[3] Center for Intelligent Sensors and MEMS, National University of Singapore, 4 Engineering Drive 3, 117576, Singapore

*Email: elelc@nus.edu.sg.

The development of flexible and stretchable electronic offers a great possibility for enabling the hybrid system with conventional silicon-based electronics. To explore the sensing and manipulation capability of self-powered flexible systems, we reported several devices include the textile-based glove and the first smart sock for monitoring human activity and enabling intuitive human machine interaction, as well as the hybrid inertial sensors and gas sensors for wearable applications. These devices not only demonstrate the diversified sensing functions for practical uses, but also become the preferable platform for the further integration of advanced techniques to realize more intelligent hybrid flexible systems.

Key words: self-powered, flexible, hybrid, sensor

INTRODUCTION

Background

The IoT has brought us a promising way to develop portable, miniaturized and multifunctional systems by integrating vast types of self-powered sensors for healthcare, biomedical detection, environmental monitoring, remote controls, and security. Among them, the hybrid electronic systems with certain flexibility are drawing a great attention of researches, as they combine both excellent functionality from the conventional silicon electronics and other components with flexible/conformable form factors. These systems can significantly facilitate the applications on deformable and wearable devices.

RESULTS

The proposed smart textile-based triboelectric nanogenerators with versatile configurations towards diversified applications including energy harvesting, internet of things (IoT), healthcare monitoring, and robotic control as illustrated in Figure 1a. The energy harvesting property of the smart textile under different motions is investigated. A multi-arch varying-height strain sensor based on the textile with a large strain sensing range from 10% to 160% is fabricated and characterized. The two-arch strain sensor then is used for finger motion detection. By leveraging this arch-shaped strain sensor on human fingers, we can successfully monitor finger motions aiming at applications of hand gesture detection for American Sign Language translation and robotic control. Besides, four self-powered sensors based on the smart textiles are fabricated and attached to different parts of the human body for activity monitoring. Together they are able to detect activities such as standing up, walking, running, arm bending, a sudden fall, and sitting. In addition, the smart textile can also be used for CO_2 sensing with the PEI coating, and a wearable arch-shaped CO_2 sensor based on the smart textile on top of a finger is developed.

Self-Powerd Intuitive Glove-Based HMI

A minimalist design based on the triboelectric nanogenerators in two configurations is proposed to balance the requirement on the full functionality and the easy to hands-on operation scheme as shown in Figure 1b. We have successfully demonstrated using the glove-based interface to control an aircraft in a shooting minigame. We have also controlled a real toy car run at all the directions on the ground wirelessly with different speeds through controlling the bending angles or the contacting forces. Similarly, a drone is also successfully controlled to fly and move in the 3D space with two more sensors embedded. With the additional sensors endowed with other defined functions, the expanded glove-based interface has also been demonstrated to mimic the same function of a mouse. Benefit from the minimalist design, this glove-based control interface could be easily produced in large scale due to the simplified device structure and its low-cost fabrication process.

Self-Powered Smart Sock for Healthcare and IoT

A self-powered and self-functional sock (S2-sock) based on TENG textile with the integration of piezoelectric sensor, as illustrated in Figure 1c. As a

self-powered sock, except the basic energy harvesting function, a facile fully coated sock can generate the featured waveforms which offer the convenient method for walking pattern recognition and motion tracking of individuals for home care applications. To be more specific, a continuous Parkinson's Disease monitoring can be realized as a complementary way of diagnosis for the routine clinic evaluation. Secondly , as a concept of sensor fusion, a quick evaluation of sweat level was also demonstrated by TENG + PZT sensor through the output generated from direct mechanical contact, since the TENG output will experience the degradation during sweating. However, the encapsulated PZT chip will not be affected by sweat and can be utilized as reference sensor to define the absolute value of decay. Moreover, the modified multi-sectional PEDOT:PSS pattern enable the gait sensing by four TENG sensors. The embedded thin PZT chips can also perform contact force analysis for specific locations. In general, this smart sock shows the great potential to be applied for healthcare and IoT applications.

Self-powered Hybrid 3D Activity Inertial Sensor

A self-powered 3D activity inertial sensor (3DAIS) is proposed for multi-axis acceleration and rotation inertial sensing in Figure 1d. The 3DAIS consists of magnetic buckyballs encapsulated inside a 3D–printed spherical shell, with multilayers of PTFE, PVDF and Al films fabricated on the inner walls of the shell and wire coils winded on the outside. The device demonstrated good performance in hand motion recognition and human activity state monitoring application. When operating as a 6-axis inertial sensor, the 3DAIS is able to sense X, Y and Z-acceleration during linear motion as well as detect roll, pitch and yaw angular velocity during rotational motion. The device possesses self-powering ability as well and is able to harvest energy through hybrid mechanisms of piezoelectric, electromagnetic and triboelectric from various energy sources such as 3D vibration, rotation and human motion, etc. The proposed 3DAIS can potentially pave the way to an advance motion sensing system with self-powering capability for wearables and healthcare telemedicine applications.

CONCLUSION

Base on the proposed devices, we successfully realized the diversified self-powered sensing functions for environmental monitoring, healthcare, human-machine interaction etc. These hybrid flexible devices are showing the unique advantages of promoting the development of intelligent wearable devices.

ACKNOWLEDGEMENTS

This work was supported by HIFES Seed Funding-2017-01 grant (R-263-501-012-133) "Hybrid Integration of Flexible Power Source and Pressure Sensors" at the National University of Singapore; Agency for Science, Technology and Research (A*STAR), Singapore and Narodowe Centrum Badań iRozwoju (NCBR), Poland Joint Grant (R-263-000-C91-305) "Chip-Scale MEMS Micro-Spectrometer for Monitoring Harsh Industrial Gases".

REFERENCES

[1] T. He, Q. Shi, H. Wang, F. Wen, T. Chen, J. Ouyang, and C. Lee, Beyond energy harvesting - multi-functional triboelectric nanosensors on a textile, Nano Energy, vol. 57, pp.338-352, 2019.

[2] T. He, Z. Sun, Q. Shi, M. Zhu, D. V. Anaya, M. Xu, T. Chen, M. R. Yuce, A. V. Thean, and C. Lee, Self-powered Glove-based Intuitive Interface for Diversified Control Applications in Real/Cyber Space, Nano Energy, vol. 58, pp.641-651, 2019.

[3] Q. Shi, C. Qiu, T. He, F. Wu, M. Zhu, J. A. Dziuban, R. Walczak, M. R. Yuce, and C. Lee, Triboelectric single-electrode-output control interface using patterned grid electrode, Nano Energy, vol. 60, pp.545-556, 2019.

[4] M. Zhu, Q. Shi, T. He, Z. Yi, Y. Ma, B. Yang, T. Chen, and C. Lee, Self-Powered and Self-Functional Cotton Sock Using Piezoelectric and Triboelectric Hybrid Mechanism for Healthcare and Sports Monitoring, ACS Nano, vol. 13, no. 2, pp. 1940-1952, 2019.

[5] K. H. Koh, Q. Shi, S. Cao, D. Ma, H. Y. Tan, Z. Guo, and C. Lee, A Self-Powered 3D Activity Inertial Sensor Using Hybrid Sensing Mechanisms, Nano Energy, vol. 56, pp. 651-661, 2019.

3C-SiC/Si technology platform for resonant MEMS sensors

Toan Dinh[1,*], Thanh Nguyen[1], Hoang-Phuong Phan[1], Pablo Guzman Duran[1], Tuan-Khoa Nguyen[1], Nam-Trung Nguyen[1] and Dzung Viet Dao[1,2]
[1]Queensland Micro and Nanotechnology Centre, Griffith University, Queensland, AUSTRALIA
[2]School of Engineering and Built Environment, Griffith University, Queensland, AUSTRALIA
*Email: toan.dinh@griffith.edu.au

The capability of growing large-area wafers of high-quality 3C-SiC on a silicon substrate makes 3C-SiC/Si a suitable technology platform for low-cost high-performance resonant sensors. We report on the characterization of 3C-SiC resonators towards tunable resonant frequency response by electrothermal coupling. In addition, we successfully demonstrate the operation of resonant 3C-SiC/Si sensors with high sensitivity and at low power consumption. Our technology platform can be employed to develop a wide range of resonant MEMS sensors with high performance and low power consumption.

Key words: Electrothermal tuning, resonant MEMS sensors, cubic silicon carbide.

INTRODUCTION

Single crystalline cubic silicon carbide (3C-SiC) is a promising material for resonant sensors thanks to its large energy bandgap and high Young's modulus. These properties make 3C-SiC suitable for high-frequency and high-quality-factor applications [1]. Recently, 3C-SiC has been successfully grown on large area of silicon (Si) substrates for low cost MEMS sensors [2]. Subsequently, the sensing effects of 3C-SiC including piezoresistance [3] and thermoresistance [4] have been intensively investigated for mechanical and thermal sensors [5, 6]. However, the use of 3C-SiC/SiC for resonators and resonant sensors is limited due to the low quality of the SiC film, especially towards high sensitivity and low power consumption.

In this work, we demonstrate the SiC/Si technology platform for tunable SiC resonators and resonant MEMS sensors with high performance and low power consumption.

RESULTS

200 nm-thick single crystalline 3C-SiC was grown on a p-type (100) Si substrate by low pressure chemical deposition (LPCVD) at a temperature of 1000°C. The high crystalline quality of 3C-SiC films was confirmed using X-ray diffraction (XRD), Selected area electron diffraction (SAED), and transmission electron microscopy (TEM). Figure 1 shows the fabrication process with 5 main steps for SiC resonators and resonant sensors.

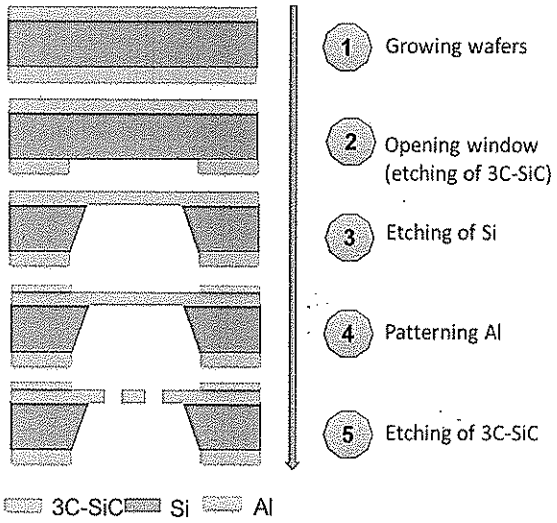

Figure 1: Fabrication process

Figure 2(left) shows the experiment setup and tuning concept of SiC resonators using electrothermal input. Figure 2(right) illustrates the photograph of the as-fabricated SiC device

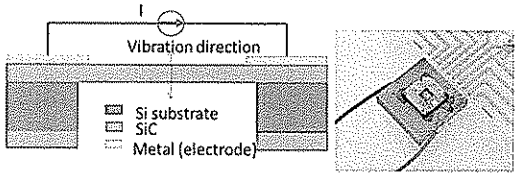

Figure 2: Schematic sketch of experiment (left) and the as-fabricated SiC device (right)

Figure 3 shows the measured resonant frequency of 72.344 kHz for the SiC bridge. Figure 4 shows the tuning resonant frequency with a tuning range of 0-80% for a current input of 0-4 mA. This indicates the potential of using the SiC resonators for highly sensitive thermal sensing applications.

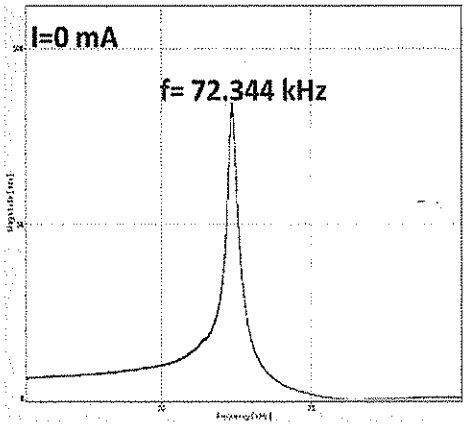

Figure 3: Measured resonant frequency at zero supplied current.

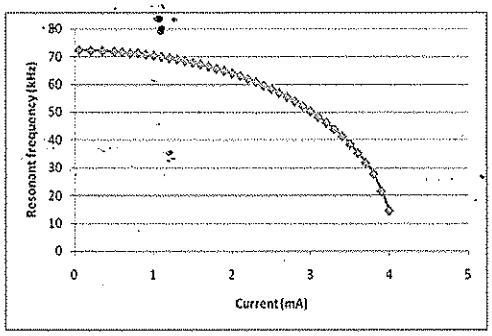

Figure 4: Tuning frequency response of SiC resonators by applied current.

Figure 5 shows the schematic sketch of an as-fabricated accelerometer using SiC as a sensing element. A constant current was applied to the SiC piezoresistor while the output voltage was measured using a lock-in amplifier. Figure 6 shows the linear increase in the measured output voltage with increasing acceleration. A sensitivity of 14.476 mV/g was measured for the sensor at a low power consumption of below 1 mW. In addition, the sensor can work in a very low power consumption mode of 1 nW (e.g. 0.1 μA supply current).

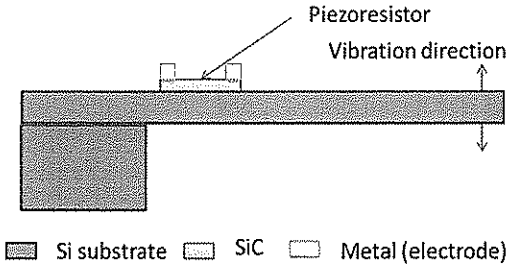

Figure 5: Schematic sketch of a SiC accelerometer.

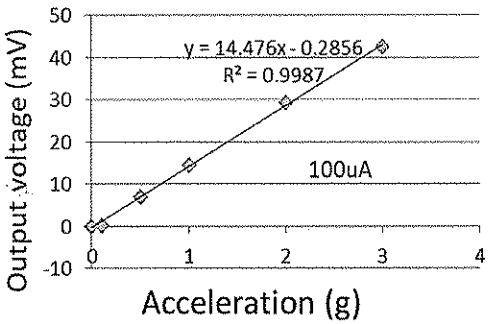

Figure 6: Output voltage vs acceleration.

CONCLUSION

We successfully demonstrate tenable frequency response of SiC resonators using electrothermal input of tunning currents. We also develop highly sensitive resonant SiC/Si sensors with low power consumption. The results indicate the potential of using our SiC/Si technology platform for resonant MEMS sensors with high performance and low power consumption.

REFERENCES

[1] K. Brueckner *et al.*, "Micro-and nano-electromechanical resonators based on SiC and group III-nitrides for sensor applications," *physica status solidi (a),* vol. 208, no. 2, pp. 357-376, 2011.

[2] L. Wang *et al.*, "Growth of 3C–SiC on 150-mm Si (100) substrates by alternating supply epitaxy at 1000 C," *Thin solid films,* vol. 519, no. 19, pp. 6443-6446, 2011.

[3] A. R. Md Foisal *et al.*, "Pushing the limits of piezoresistive effect by optomechanical coupling in 3C-SiC/Si heterostructure," *ACS applied materials & interfaces,* vol. 9, no. 46, pp. 39921-39925, 2017.

[4] T. Dinh *et al.*, "Unintentionally doped epitaxial 3C-SiC (111) nanothin film as material for highly sensitive thermal sensors at high temperatures," *IEEE Electron Device Letters,* vol. 39, no. 4, pp. 580-583, 2018.

[5] V. Balakrishnan, T. Dinh, H.-P. Phan, D. V. Dao, and N.-T. Nguyen, "Highly sensitive 3C-SiC on glass based thermal flow sensor realized using MEMS technology," *Sensors and Actuators A: Physical,* vol. 279, pp. 293-305, 2018.

[6] A. Qamar *et al.*, "The effect of device geometry and crystal orientation on the stress-dependent offset voltage of 3C–SiC (100) four terminal devices," *Journal of Materials Chemistry C,* vol. 3, no. 34, pp. 8804-8809, 2015.

WAFER TO WAFER BONDING FOR MEMS MANUFACTURING

Guenter Pauzenberger
Regional Asia / Pacific Sales and Marketing, EV Group
*Email: G.Pauzenberger@evgroup.com

Wafer bonding is one of the enabling technology for MEMS (Micro Electro Mechanical Systems), MOEMS (Micro Optical Electro Mechanical Systems), 3DICs (3D Integrated Circuits), BSI (Back Side Illuminated Image Sensor), CIS (CMOS Image Sensors), SOI wafers, heterogeneous integration, multi junction PV (Photo Voltaic) cells, high performance RF (Radio Frequency) filters, microfluidics and wafer level optics. It enables heterogeneous integration and the continuous reduction of device size.

This presentation will highlight the often hidden process of wafer bonding by reviewing the primary aligned wafer bonding processes for MEMS and 3DICs for both homogeneous and heterogeneous integration. The bonding processes reviewed will focus on metal based wafer to wafer bonding including solder/ eutectic bonding, thermo-compression bonding, plasma activated direct bonding and hybrid bonding.

"MSS" TOWARDS ARTIFICIAL OLFACTION

Genki Yoshikawa[1,*]
[1]National Institute for Materials Science
*Email: YOSHIKAWA.Genki@nims.go.jp

"Membrane-type Surface stress Sensor (MSS)" is a kind of nanomechanical sensors, which have potential as a versatile sensing platform, especially for artificial olfaction. MSS detects surface stress induced by sorption of gas molecules on a receptor layer coated on the surface of MSS. An array of MSS with various receptor layers gives multidimensional sensing signals, which provide patterns of target gases. To establish practical artificial olfaction, various components including receptor layers and multidimensional data analysis techniques have been developed, optimized, and integrated.

Key words: MSS, artificial olfaction, olfactory sensor

INTRODUCTION

Background

The development of practical olfactory sensors has been expected in many fields such as agriculture, medicine, safety, and environment.

MSS

Yoshikawa *et al.* focused on a nanomechanical sensor as a candidate for a versatile sensing platform, and performed optimization based on the material characteristics and structural mechanics of the sensor element, leading to the development of "Membrane-type Surface stress Sensor (MSS)" (Fig. 1) [1]. Owing to its unique structure, MSS achieved more than 100 times higher sensitivity compared to a conventional piezoresistive cantilever sensor [1, 2]. MSS has the following characteristics required to realize a practical olfactory sensor: high sensitivity, small size, versatility, room temperature operation, stability, low power consumption, and quick response.

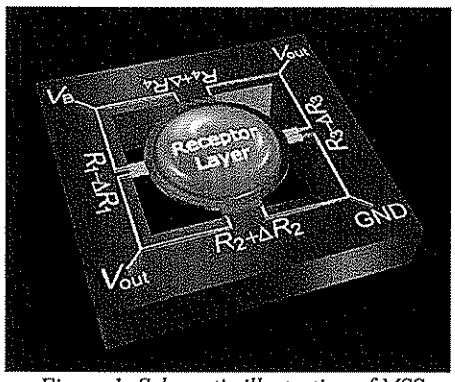

Figure 1: Schematic illustration of MSS.

DEVELOPMENTS

Analytical models for a receptor layer

It has been confirmed that almost all materials, including organic materials, inorganic materials, and biomaterials, can be used as a receptor material for MSS. To provide a guideline for effective receptor layers, we developed an analytical model (Yoshikawa [3]) and a parameter estimation protocol based on viscoelastic model (Imamura *et al.* [4]).

Functional materials for effective receptor layers

As actual effective sensing materials, we developed, for example, functional nanoparticles (Shiba *et al.* [5-8]) and a porphine-based humidity-resistant material (Ngo *et al.* [9]). We also succeeded in demonstrating "pattern recognition of solid material" by focusing on "solid-gas interaction" (Minami *et al.* [10]).

APPLICATIONS

Identification of various gas samples

Various targets have been measured so far as potential applications of MSS-based olfactory sensors. Imamura *et al.* demonstrated the identification of spices and herbs as an example of food identification [11]. Loizeau and Lang *et al.* demonstrated different sensor signal patterns for exhaled breath samples collected from head and neck cancer patients and healthy persons [12]. In addition, Lang *et al.* reported changes in signal patterns before and after surgery of cancer [13]. Minami *et al.* demonstrated detection of volatile organic compounds included in body odor [14]. Although MSS has been expected as a sensing platform which contributes to medical diagnosis and healthcare, for practical application in the actual medical field, basic research based on large number of samples is still required. We have been carrying on the development of basic technology/protocol with careful verification in collaboration with hospitals.

Integration with machine learning

The application scope of multidimensional data obtained through odor measurements can be further expanded by machine learning. As an example of specific information extraction, Shiba and Tamura *et al.* succeeded in quantitative prediction of "alcohol content" from various liquor odors by combining MSS, functional nanoparticles, and machine learning [7]. Furthermore, applying this approach, the concentration of each component in the ternary

mixture was successfully quantified [15]. Recently, Imamura *et al.* demonstrated "free-hand" gas identification by integrating transfer function concept with MSS and machine learning [16].

CONCLUSION

We have been developing the MSS and related technologies. To implement the olfactory sensor system in society, however, it is also required to integrate and optimize various technologies with industry. To this end, an industry-academia-government collaboration called the "MSS Alliance" was launched in September 2015. In addition, the MSS Forum was established in November 2017 to encourage interested companies/organizations to perform demonstration experiments (https://mss-forum.com). Currently, more than 50 members, including companies, universities and research institutes, are participating in this project.

ACKNOWLEDGEMENTS

We thank all the members and collaborators involved in the projects. These works and projects were supported by various funding, including JST CREST (JPMJCR1665); a Grant-in-Aid for Scientific Research (A), 18H04168, MEXT, Japan; the Public/Private R&D Investment Strategic Expansion Program (PRISM), Cabinet Office, Japan; the Center for Functional Sensor & Actuator (CFSN), NIMS; and the World Premier International Research Center Initiative (WPI) on Materials Nanoarchitectonics (MANA), NIMS.

REFERENCES

[1] G. Yoshikawa, T. Akiyama, S. Gautsch, P. Vettiger, H. Rohrer, "Nanomechanical Membrane-type Surface Stress Sensor," ***Nano Letters*** **11**, 1044-1048 (2011).

[2] G. Yoshikawa, T. Akiyama, F. Loizeau, K. Shiba, S. Gautsch, T. Nakayama, P. Vettiger, N. F. de Rooij, M. Aono, "Two Dimensional Array of Piezoresistive Nanomechanical Membrane-Type Surface Stress Sensor (MSS) with Improved Sensitivity," ***Sensors*** **12**, 15873-15887 (2012).

[3] G. Yoshikawa, "Mechanical analysis and optimization of a microcantilever sensor coated with a solid receptor film," ***Applied Physics Letters*** **98**, 173502 (2011).

[4] G. Imamura, K. Shiba, G. Yoshikawa, T. Washio, "Analysis of nanomechanical sensing signals; physical parameter estimation for gas identification," ***AIP Advances*** **8**, 075007 (2018).

[5] K. Shiba, T. Sugiyama, T. Takei, G. Yoshikawa, "Controlled growth of silica-titania hybrid functional nanoparticles through a multistep microfluidic approach," ***Chemical Communications*** **51**, 15854-15857 (2015).

[6] K. Shiba, T. Takei, G. Yoshikawa, M. Ogawa, "Deposition of a titania layer on spherical porous silica particles and their nanostructure-induced vapor sensing properties," ***Nanoscale*** **9**, 16791-16799 (2017).

[7] K. Shiba, R. Tamura, G. Imamura, G. Yoshikawa, "Data-driven nanomechanical sensing: specific information extraction from a complex system," ***Scientific Reports*** **7**, 3661 (2017).

[8] K. Shiba, R. Tamura, T. Sugiyama, Y. Kameyama, K. Koda, E. Sakon, K. Minami, H. T. Ngo, G. Imamura, K. Tsuda, G. Yoshikawa, "Functional Nanoparticles-Coated Nanomechanical Sensor Arrays for Machine Learning-Based Quantitative Odor Analysis," ***ACS Sens*** **3**, 1592-1600 (2018).

[9] H. T. Ngo, K. Minami, G. Imamura, K. Shiba, G. Yoshikawa, "Effects of Center Metals in Porphines on Nanomechanical Gas Sensing," ***Sensors (Basel)*** **18**, 1640 (2018).

[10] K. Minami, G. Imamura, T. Nemoto, K. Shiba, G. Yoshikawa, "Pattern recognition of solid materials by multiple probe gases," ***Materials Horizons***, 10.1039/c1038mh01169a (2019).

[11] G. Imamura, K. Shiba, G. Yoshikawa, "Smell identification of spices using nanomechanical membrane-type surface stress sensors," ***Japanese Journal of Applied Physics*** **55**, 1102B1103 (2016).

[12] F. Loizeau, H. P. Lang, T. Akiyama, S. Gautsch, P. Vettiger, A. Tonin, G. Yoshikawa, C. Gerber, N. d. Rooij, "Piezoresistive Membrane-Type Surface Stress Sensor Arranged in Arrays for Cancer Diagnosis through Breath Analysis," ***MEMS 2013***, 621-624 (2013).

[13] H. P. Lang, F. Loizeau, A. Hiou-Feige, J. P. Rivals, P. Romero, T. Akiyama, C. Gerber, E. Meyer, "Piezoresistive Membrane Surface Stress Sensors for Characterization of Breath Samples of Head and Neck Cancer Patients," ***Sensors (Basel)*** **16**, 1149 (2016).

[14] K. Minami, K. Shiba, G. Yoshikawa, "Discrimination of structurally similar odorous molecules with various concentrations by using a nanomechanical sensor," ***Analytical Methods*** **10**, 3720-3726 (2018).

[15] K. Shiba, R. Tamura, T. Sugiyama, Y. Kameyama, K. Koda, E. Sakon, K. Minami, H. T. Ngo, G. Imamura, K. Tsuda, G. Yoshikawa, "Functional nanoparticles-coated nanomechanical sensor arrays for machine learning-based quantitative odor analysis," ***ACS Sensors*** **3**, 1592-1600 (2018).

[16] G. Imamura, K. Shiba, G. Yoshikawa, T. Washio, "Free-hand gas identification based on transfer function ratios without gas flow control," ***Scientific Reports*** **9**, 9768 (2019).

ARTIFICAL OLFACTION BASED ON TRANSFER FUNCTION RATIOS

Gaku Imamura[1,2*], Kota Shiba, Genki Yoshikawa[1,2,3], Takashi Washio[4]
[1]International Center for Materials Nanoarchitectonics(MANA), National Institute for Materials Science (NIMS); [2]Center for Functional Sensor & Actuator (CFSN), NIMS;
[3]Materials Science and Engineering, Graduate School of Pure and Applied Science, University of Tsukuba
[4]The Institute of Scientific and Industrial Research, Osaka University
*Email: IMAMURA.Gaku@nims.go.jp

Artificial olfaction has been attracting much attention because of its potential applications in various fields. To realize a practical artificial olfaction, gas flow control is one of the most important issues because signal features which are effective in gas identification can be obtained only from measurements in which gas flow rates are strictly controlled. To resolve this issue, we have developed a gas identification method based on transfer function ratios (TFRs), which are intrinsic to the combination of sensors and gas species. As TFRs can be calculated only from the sensing signals, gas species can be identified without controlling or monitoring gas flow rates. Using membrane-type surface stress sensors (MSS), we developed a gas identification system, in which samples are measured by manually moving a MSS chip. With this system, we demonstrated odor identification of three spices with an accuracy of 0.89±0.04.

Key words: sensors, artificial olfaction, machine learning, IoT device

INTRODUCTION

Background

Olfaction is the only sense that has not been realized as a practical sensor. One of the difficulties associated with practical artificial olfaction is analysis on sensor data obtained through measurements. In a typical artificial olfactory system using multiple chemical sensors, odors—complex mixtures of gases—are delivered to sensors by controlling flow rates with pumps or mass flow controllers. From the sensor data obtained through such measurements, features that are characteristic in each odor (*e.g.* intensity, slope, decay constant) is extracted for identification.[1] In such typical measurements, gas flow rates must be fixed for every measurement; otherwise, data cannot be compared with each other. Such constraint in measurements has severely limited the implementation of artificial olfactory system.

To resolve this issue, we have developed a data analysis method based on transfer function ratios (TFRs). As TFRs can be calculated only from sensing signals from gas sensor array, gas identification without any gas flow control is realized. In this study, we have developed a gas measurement system using membrane-type surface stress sensors (MSS)—newly developed MEMS-based sensors that detect surface stress induced by gas sorption—as gas sensors to demonstrate the *free-hand measurement*, in which gases are measured by simply moving an MSS chip near a sample (Fig.1). From the data obtained with this system, we developed a machine learning models that identify odors of samples. The present approach for gas identification protocol will contribute to realization of practical artificial olfaction.[2]

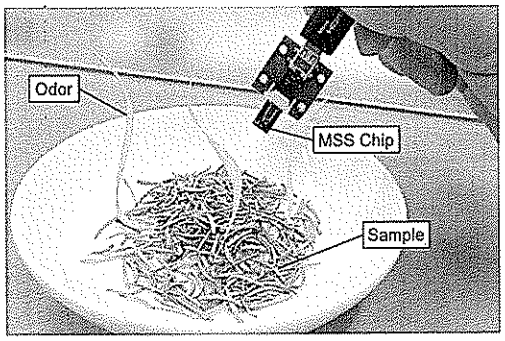

Figure 1: Free-hand measurement on a sample with an MSS chip.

Transfer function ratios

When the response of a gas sensor to a gas input is regarded to be linear, the sensor response $y(t)$ can be described by the convolution of gas input pattern $x(t)$ and time-domain transfer function $h_g(t)$:

$$y(t) = \int_0^t h_g(\tau)x(t-\tau)d\tau \qquad (1)$$

In the frequency-domain, Equation (1) can be written as the following form:

$$Y(f) = H_g(f)X(f) \qquad (2)$$

where $X(f)$, $Y(f)$, and $H_g(f)$ are frequency-domain expressions for $x(t)$, $y(t)$, and $h_g(t)$. Assuming that each channel of a gas sensor array shows a different sensing property and is in close proximity with each other, $X(f)$ can be considered to be the same for every channel. Then, the following equation holds for arbitrary channels m and n.

$$X(f) = \frac{Y_m(f)}{H_{g,m}(f)} = \frac{Y_n(f)}{H_{g,n}(f)} \quad (3)$$

Let $K_{m,n}(f)$ be defined as $K_{m,n}(f) = Y_m(f)/Y_n(f)$, $K_{m,n}(f)$ can be described as the following form from Equation (3):

$$K_{m,n}(f) = \frac{Y_n(f)}{Y_m(f)} = \frac{H_{g,n}(f)}{H_{g,m}(f)} \quad (4)$$

Equation (4) indicates that $K_{m,n}(f)$ is the transfer function ratio (TFR); that is, the ratio of transfer function of channel n to that of channel m. It should be noted that $K_{m,n}(f)$ is intrinsic to the combination of sensors and gas species and can be calculated only from the sensing signals, indicating that neither control nor monitor of gas input patterns is needed.

RESULTS

As TFRs can be calculated only from the sensor signals from a gas sensor array, gas species can be identified without any gas flow control units. To demonstrate gas identification through the free-hand measurement, we developed a gas measurement system utilizing MSS as gas sensors. The MSS chip contains four channels, each of which exhibits different sensing property. The odors of the spices were measured by freely moving the MSS sensor chip near the samples as shown in Fig.1.

Based on the measurement data obtained through the free-hand measurements, we calculated TFRs for each spice. The results of the principal component analysis (PCA) are shown in Fig.2. Each data point represents TFRs calculated from segmented measurement data. Three clusters according to the spices are formed on the PC planes, indicating that TFRs reflect the different chemical interaction between the sensor channels and odors. From the dataset of TFRs, we developed a machine learning model to identify the odors. Using random forest as a classifier, we achieved a classification accuracy of 0.89±0.04.

CONCLUSION

We have developed a signal analysis method based on TFRs, which can be calculated only from sensing signals from an array of chemical sensors without the information of gas input patterns. Combined with MSS—miniaturized gas sensors fabricated by MEMS techniques, we demonstrated odor identification of spices through the free-hand measurement without using any gas flow control units such as pumps or mass flow controllers. The present study can realize compact artificial olfaction that people without specific expertise can use, leading to practical artificial olfaction.

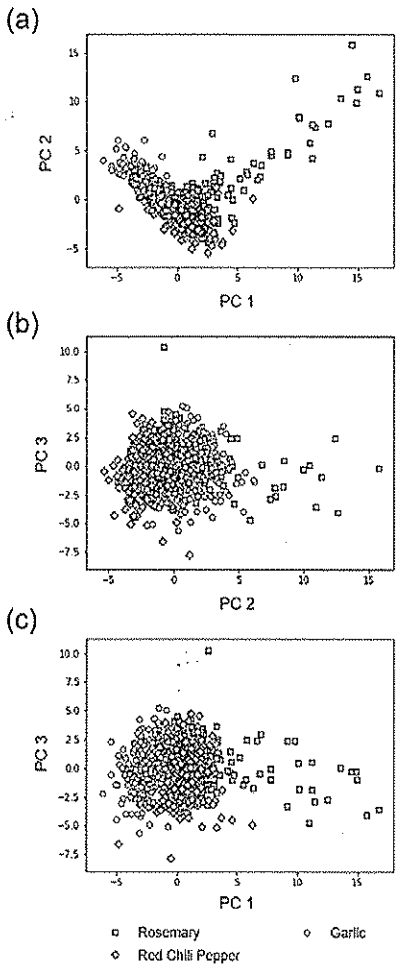

Figure 2: PCA scatter plot of TFRs calculated from the free-hand measurements on the spices.

ACKNOWLEDGEMENTS

This work was supported by the Leading Initiative for Excellent Young Researchers, Ministry of Education, Culture, Sports, Science and Technology (MEXT), Japan; a Grant-in-Aid for Young Scientists, 18K14133, MEXT, Japan; JST CREST (JPMJCR1665 and JPMJCR1666); a Grant-in-Aid for Scientific Research (A), 18H04168, MEXT, Japan; the Public/Private R&D Investment Strategic Expansion Program (PRISM), Cabinet Office, Japan; the Center for Functional Sensor & Actuator (CFSN), NIMS; the World Premier International Research Center Initiative (WPI) on Materials Nanoarchitectonics (MANA), NIMS; and the MSS Alliance.

REFERENCES

[1] G. Imamura, K. Shiba, and G. Yoshikawa "Smell identification of spices using nanomechanical

membrane-type surface stress sensors" *Japanese Journal of Applied Physics*, 55, 1102B3 (2016).

[2] G. Imamura, K. Shiba, and G. Yoshikawa, and T. Washio "Free-hand gas identification based on transfer function ratios without gas flow control" *Scientific Reports*, 9, 9768 (2019).

PATTERN RECOGNITION OF SOLID MATERIALS BY MULTIPLE PROBE GASES

Kosuke Minami
Center for Functional Sensor & Actuator (CFSN)
National Institute for Materials Science (NIMS)
1-1 Namiki, Tsukuba, Ibaraki 305-0044 Japan

A pattern recognition-based chemical sensor array is an efficient approach to discriminating odors or a complex mixture of gaseous molecules. In such an approach, solid materials are coated on surfaces of sensors as probe receptors, and gaseous molecules are exposed to those sensors as targets. Here, we propose the reverse approach, that is, gaseous molecules as probes and solid materials as targets, leading to pattern recognition of solid materials [1]. Using a nanomechanical sensor as an example of a sensing platform, we have demonstrated that this approach can discriminate polymers with different molecular weights as well as those having slightly different functional groups evaluated through detailed classification using a support vector machine in addition to principal component analysis and linear discriminant analysis. Classification of those target solid materials with 100% accuracy has been achieved with some specific combinations of probe gases. Since any kind of gaseous molecule and any kind of chemical sensor can be utilized as the probe and sensing platform, respectively, this study will open a new world for comprehensive analysis of solid materials through a pattern formed by the gas–solid interaction.

References

[1] Minami, K.; Imamura, G.; Nemoto, T.; Shiba, K.; Yoshikawa, G. *Materials Horizons* **2019**, *6*, 580–586.

MEMS-BASED PIEZORESISTIVE SENSORS FOR HEALTHCARE AND INFRASTRUCTURE MONITORING

Thanh-Vinh Nguyen*
Sensing Systems Research Center,
National Institute of Advanced Industrial Science and Technology (AIST), JAPAN
*Email: vinh.nguyen@aist.go.jp

We have developed MEMS-based force sensors for applications of healthcare and monitoring of infrastructure. These sensors consist of ultrathin piezoresistive cantilevers and fluid (air or liquid) chambers. When the chamber is filled with air, the sensor becomes a highly sensitive and robust differential pressure sensor that can measure the blood pulse wave. On the other hand, when the chamber is filled with liquid, the sensor becomes a wide range vibration sensor which can cover the frequency range of an accelerometer and an AE sensor. Therefore, the proposed sensors are suitable for the applications of wearable blood pressure monitoring and infrastructure health monitoring.

Key words: MEMS, force sensors, fluid chambers, blood pulse wave, bridge monitoring

INTRODUCTION

Blood pulse wave sensor

Measuring blood pulse waves can provide significant information about vascular diseases, such as diabetes, arteriosclerosis in a human body, and heart failure. To evaluate healthiness, Pulse Wave Velocity (PWV), which is related to the blood pressure and arterial stiffness, has been used as an indicator for diagnostics of some diseases including diabetes as shown in previous researches [2]. PWV is defined by the following equation using pulse waves measured at two points:

$$PWV = d/\Delta t$$

where d is the distance of two measurement points and Δt is the pulse transit time (PTT), which is the time delay for the pulse wave to transmit between two measurement points on the blood vessel.

In this study, we propose a sensor that can measure pulse waves with high sensitivity by only placing on human skin without additional pressing force against human skin (Figure 1) [1]. The sensor consists of a chamber covered with a thin elastic film and a cantilever which can measure pressure change of the chamber. During the measurement, the membrane of the air chamber is pressed against human skin above a blood vessel. The radius of the vessel is changed due to the blood flow, and the membrane deforms according to the deformation of the skin. The deformation of the membrane results in pressure change of the chamber, which is directly measured by the cantilever. Due to the high sensitivity of the cantilever to differential pressure and the flexibility of the membrane [8], the sensor is able to detect the pulse waves even when the sensor is only placed on the skin above the blood vessel.

Wide band vibration sensor for structural monitoring

Structural monitoring of infrastructures such as bridges, tunnels, and dams is important for ensuring the safety of these structures. The vibrational properties of a deteriorated infrastructure change depending on the deterioration stage. At the beginning stage of deterioration, microscale cracks occur, resulting in the irreversible changes in internal structure. During this stage, it is known that acoustic emission (AE) occurs, resulting in the vibrations whose frequencies are in the range of tens kHz to MHz. As the cracks propagate and become wider, the vibration frequency decreases. At the final stage prior to the collapse of the structure, vibrations at the low frequency (less than 100 Hz) can be observed.

As one of the approaches to develop a sensor that can measure vibration in a wide range of frequency (from several Hz to MHz), a sensor design with a piezoresistive beam placed at liquid/air interface was proposed. These sensors can measure vibration whose frequency is from several Hz to MHz by utilizing the effect of surface tension wave. However, this sensor design has a crucial issue that the liquid can leak through the gap surrounding the sensing beam, causing a dramatic reduction of the sensor's sensitivity. Therefore, to improve the durability of the sensor, a structure that can prevent liquid leakage is required.

Here, we propose a sensor design that inherits the advantage of wide frequency band from previous liquid on piezoresistive beam structure and is able to prevent the liquid leakage (Figure 2) [2]. Basically, in the proposed device, a thin Parylene film is deposited to completely cover the beam, leaving no gap for liquid to leak. Moreover, in the proposed device, not only the flat Parylene membrane but also the ones with corrugated patterns can be fabricated. These

patterns make the membrane softer and are expected to increase the sensitivity of the sensor.

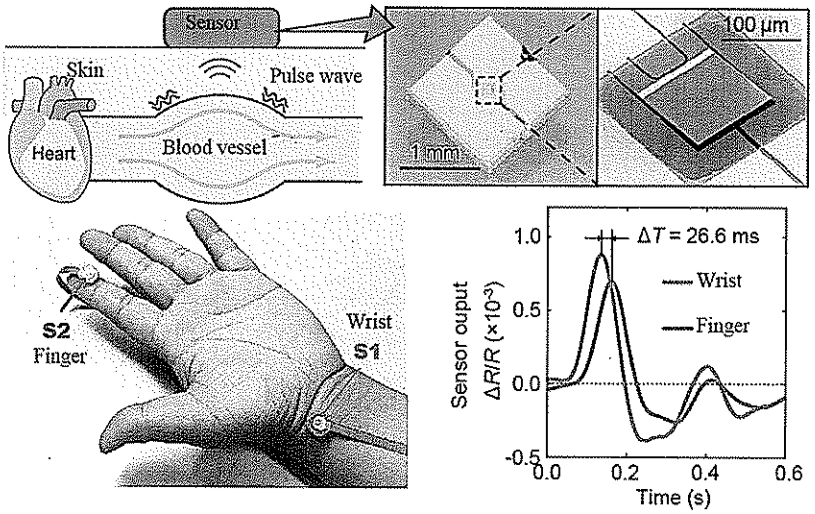

Figure 1: MEMS-based force sensor for blood pulse wave measurement.

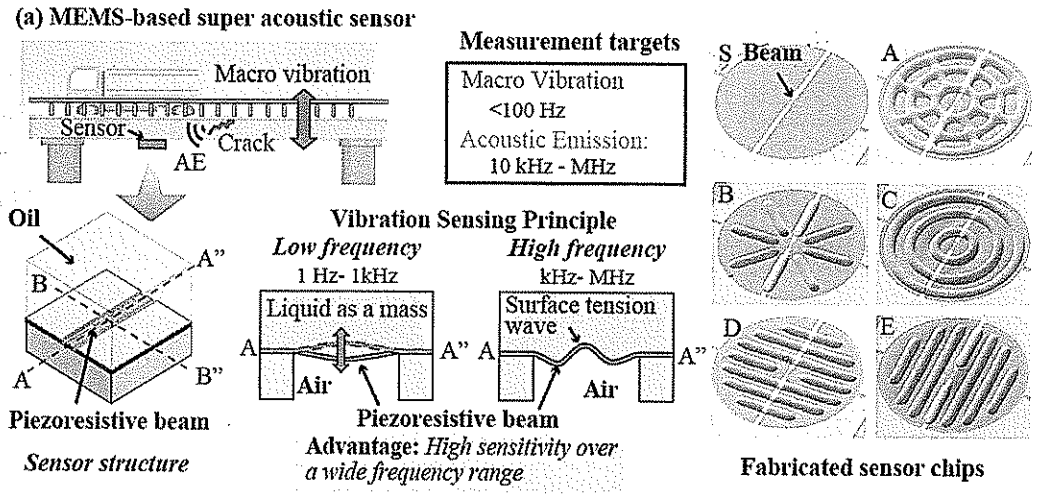

Figure 2: MEMS-based wide range vibrational sensor for infrastructure health monitoring.

ACKNOWLEDGEMENTS

The photolithography masks were made using the University of Tokyo VLSI Design and Education Center (VDEC)'s 8 inch EB writer F5112 + VD01 donated by ADVANTEST Corporation. This work was supported by JSPS KAKENHI Grant-in-Aid for Young Scientists (A) Grant Number 17H04903.

REFERENCES

[1] R Suzuki, T-V Nguyen, T Takahata, and I Shimoyama, "A Piezoresistive Vibration Sensor with Liquid On Corrugated Membrane," *The 32nd International Conference on Micro Electro Mechanical Systems (MEMS 2019)*, pp. 688 – 691, Seoul, Korea, Jan. 27–31, 2019.

[2] Y Mizuki, T-V Nguyen, T Takahata, and I Shimoyama, "Highly sensitive pulse wave sensor with a piezoresistive cantilever inside an air chamber," *The 32nd International Conference on Micro Electro Mechanical Systems (MEMS 2019)*, pp. 611-614, Seoul, Korea, Jan. 27–31,

2019.

MEMS BASED ACOUSTIC EMISSION SENSOR

Minh-Dung Nguyen[1,*], Isao Shimoyama[2]
[1,2]Toyama Prefectural University, Toyama, Japan
*Email: jun@pu-toyama.ac.jp

This study proposes an approach to measure acoustic emission (AE) signals using ultra-thin piezoresistive beam combined with a non-vaporized liquid, which was silicone oil. The AE sensor is based on liquid-on-beam structure, in which a liquid droplet is placed on a microscale piezoresistive double-supported beam to form a multiplayer structure of liquid/beam/air.The results from experiments and demonstration of breaking pencil lead demonstrate that this structure enables the sensor to measure AE signals with high sensitivity in broad frequency range.

Key words: piezoresistive, acoustic emission, MEMS

INTRODUCTION

Background

As one of non-destructive testing methods for material degradation, acoustic emission (AE) sensors have attracted a significant amount of researches. Conventional AE sensors can be found in literature incorporating capacitive type and piezoelectric type. Generally, these types of sensor utilized the resonance of solid sensing structure, causes limited frequency range. In addition, the signal to noise ratio is supposed to decrease when the device is miniaturized. This study proposes an approach to measure AE signals in a wide frequency range, using ultra-thin piezoresistive beam combined with a non-vaporized liquid (silicone oil HIVAC F-4). The point here is the liquid-on-beam structure, in which a liquid droplet is placed on a microscale double-supported beam to form a multiplayer structure of liquid/beam/air (Fig.1). The double-supported beam was 300nm-thick and had a small air gap, which was downscaled to 1μm, to prevent liquid leak. A single beam can measure pressure vibration up to few tens kHz in air. However when it is designed at the interface of liquid and air, the measurable range becomes much wider due to the liquid surface wave phenomenon. We took advantage of this effect to propose a wide-range AE signals in this study.

RESULTS

The results from experiment using Laser Doppler Vibrometry (Polytec SMA-500) demonstrate that the sensor has a high sensitivity, due to the large displacement in a wide frequency range (Fig. 2). Fig. 3 shows the demonstration of breaking pencil lead using the proposed AE sensor. Since the AE signals were detected by the beam's resistance change, this device can be miniaturized without sensitivity decrease. Furthermore, regarding the miniaturized simple structure and the low-cost of MEMS (Micro Electro Mechanical Systems) based fabrication process, the proposed AE sensor can be expected to lead infrastructure monitoring system, which is rather difficult now due to the high-cost issue.

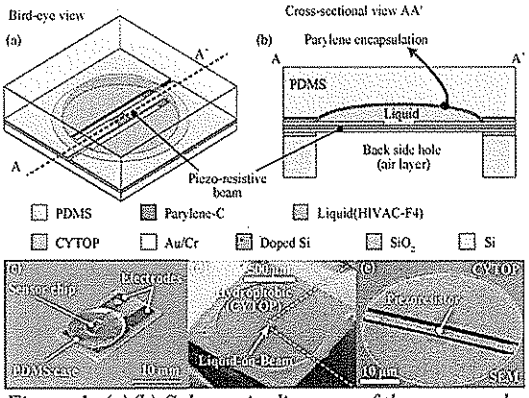

Figure 1. (a)(b) Schematic diagram of the proposed MEMS AE sensor. (c)(d)(e) Photograph and SEM images of the fabricated sensor and the SOI chip.

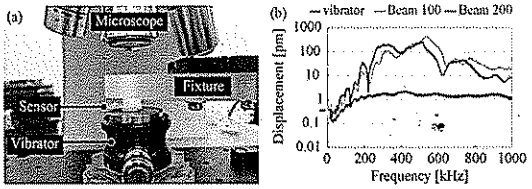

Figure 2. (a) Experimental setup for Laser Doppler Vibrometry using Polytec SMA-500 (b) Displacement of the center point of the beams in the range from 10kHz to 1MHz.

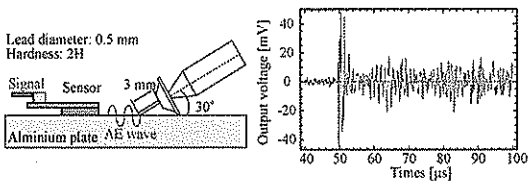

Figure 3. Demonstration of pencil lead breaking using the proposed MEMS AE sensor.

DEVELOPMENT OF MECHANICALLY-ROBUST PIEZOELECTRIC MICROMACHINED ULTRASONIC TRANSDUCER (pMUT) WITH ISLAND-SHAPED PZT MONOCRYSTALLINE THIN FILMS

Pham N. Thao, Shinya Yoshida, and Shuji Tanaka
Tohoku University, JAPAN

We proudly report on our success to develop a mechanically-robust piezoelectric micromachined ultrasonic transducer (pMUT) based on a monocrystalline Pb(Zr, Ti)O_3 thin film (Mono-PZT) for the first time. The Mono-PZT has the world-leading value of figure of merit (FOM) for pMUT. However, the conventional-design pMUT is fractured easily due to its brittle property (Fig. 1). For overcoming this drawback, we proposed a new design: island-shaped Mono-PZT structure covered with a ring-shaped polyimide thin film (Fig. 2). The fracture test proved that this design is effective for enhancing the mechanical robustness (Fig. 6). Its electromechanical coupling factor (k_{eff}^2) was also two times higher than that of the conventional design. This achievement has a great potential to create not only a higher-performance but also highly-reliable pMUT.

A COMPACT TRACE-MOISTURE SENSOR BASED ON CAVITY RING-DOWN SPECTROSCOPY

Hisashi Abe
National Metrology Institute of Japan, Tsukuba, Japan
*Email: *abe.h@aist.go.jp*

Cavity ring-down spectroscopy (CRDS) is a very powerful tool for measurement of trace species, particularly for trace moisture, because CRDS is not influenced by atmospheric moisture outside the sample cell, which is a major source of uncertainty in the measurement of trace moisture in gases. However, application of CRDS to field measurement is still limited. This is because the typical size of CRDS systems is bulky and not suitable for many on-site or in-situ measurements. In order to address this issue, we developed a compact trace-moisture sensor based on CRDS at National Metrology Institute of Japan (NMIJ).

The sensor has the dimensions of 25 cm × 20 cm × 20 cm and the mass of approximately 3 kg. The sensor unit includes ring-down cavity, fiber optic collimator, and photo diode. A continuous-wave distributed-feedback laser diode placed outside the sensor unit was connected to the collimator using an optical fiber. The SI-traceable standard gas mixture of water in nitrogen generated using a magnetic suspension balance/diffusion-tube humidity generator at NMIJ was introduced into the ring-down cavity. The laser light exited from the collimator was injected into the ring-down cavity. The ring-down signal detected with the photo diode was transferred to a digitizer. The digitized signal was transferred to a personal computer and fitted with an exponential function to obtain the ring-down time. The mole fraction of water in nitrogen inside the cavity calculated from the ring-down time was in good agreement with the standard value in the range of 10 ppb to 10000 ppb.

MOISTURE SENSOR; EARLY DETECTION OF DEW CONDENSATION

Jin Kawakita*
National Institute for Materials Science
*Email: KAWAKITA.Jin@nims.go.jp

This research work is related to finding and developing a new sensor, which can detect slight amount of small water droplet, based on the galvanic action. This sensor can be used for initial and early detection of dew condensation, which is not possible by using current technologies such as hygrometer. This sensor shows high sensitivity and quick response with a minimum detection level of 0.2 μm. This sensor is applicable to advanced detection of dew condensation in the agriculture.

Key words: dew condensation, advanced detection

INTRODUCTION

Dew condensation causes various phenomena such as corrosion of metal, fogging of glass and disease to crops. In order to suppress or prevent dew condensation, it should be detected at an initial or early stage, moreover in advance if hopeful. The conventional techniques, however, are useless for that purpose. For instance, when relative humidity (RH) reaches 100%, dew condensation must occur while a common method to estimate RH from its correlation with changes in electrical resistance or capacitance of hygroscopic polymer by absorption of water vapor in the atmosphere cannot detect occurrence of condensed dew, i.e. liquid water. Moreover, it also takes 10 seconds and more to respond to the changes in RH. On the other hand, most commercial methods of water detection by change in electrical signal between two electrodes are merely applicable to comparatively much water in visible extent grown by continuous dew condensation. NIMS has developed a sensor that detect fine and slight water with high accuracy and quick response, based on galvanic current generated by attaching water like a bridge between different metal lines with a narrow gap, as shown in Fig.1.

EXPERIMENTAL

The sensor electrodes were interdigit arrayed lines of Au and Al with 1 μm in width and 0.2 μm in thickness were opposed and inserted between mutual lines in a length of 1 mm with gaps of 0.2 to 10 μm on a silicon wafer covered with a silica layer. Electric current from the sensor electrodes was measured at a minimum interval of 0.2 sec through a device for A/D conversion of the signal from the sensor electrode. Humidity around the sensor electrodes controlled from 30% to 100% and the temperature of the sensor was changed from the ambient temperature to dew point. The microscopic observation of the surface of the sensor electrodes was carried out under the control of humidity around the sensor electrodes.

RESULTS

Current response of the sensor coincided with appearance / disappearance of water droplets on the sensor surface with a considerable accuracy. Furthermore, this sensor detected clearly water droplets under high humidity more than 80 % could be detected, which is difficult to detect with a general hygrometer. In addition, narrower gap between the sensor electrodes showed more sensitive response to smaller water droplet. Especially, the electrode with the gap of 0.5 μm also showed stepwise current response according to the changes in humidity from 60 % to 90 % presumably due to adsorption of water molecules. Recently, this sensor showed detection and distinction of dew condensation in the agricultural field better than commercial hygrometer.

SUMMARY

This sensor could detect dew condensation at an initial and early stage and moreover might predict in advance. It would be used for sensing of moisture in the environment.

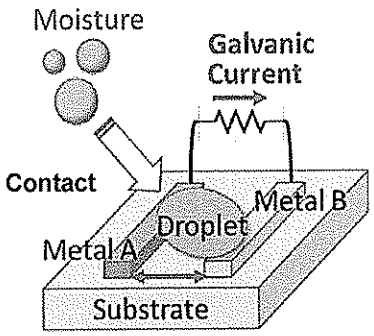

Figure 1: Working principle of Moisture Sensor

Optoelectronic coupling for ultrasensitive mechanical sensors

Thanh Nguyen[1,*], Toan Dinh[1], Hoang-Phuong Phan[1], Tuan-Khoa Nguyen[1], Abu Riduan Md Foisal[1], Nam-Trung Nguyen[1] and Dzung Viet Dao[1,2]
[1]Queensland Micro and Nanotechnology Centre, Griffith University, Queensland, AUSTRALIA
[2]School of Engineering and Built Environment, Griffith University, Queensland, AUSTRALIA
*Email: thanh.nguyen11@griffithuni.edu.au

Herein, we report optoelectronic coupling principle utilized for enhancement performance of mechanical sensors. As proof of principle, optoelectronic coupling principle was demonstrated on a 3C-SiC/Si heterojunction structure pressure sensor. By applying the optoelectronic coupling principle, the sensitivity of the pressure sensor can be improved five order of magnitude. A sensitivity of approximately 0.87 kPa^{-1} was observed, which is the most sensitive semiconductor-based pressure sensor to date. Consequently, our findings can be deployed to develop ultra-sensitive mechanical sensors and MEMS/NEMS sensing applications.

Key words: Optoelectronic coupling, ultra-sensitive pressure sensor, piezoresistive effect.

INTRODUCTION

Pressure sensors are considered as one of the most prominent microelectromechanical system (MEMS) devices [1] with diverse applications in robotics, medicine [2, 3], automobile industry [4], homeland security [5], energy harvesting [6] and environmental monitoring [2, 5].

It is desirable to enhance the performance of piezoresistive pressure sensors, particularly in sensitivity, durability, reliability, linearity, and respond time. To date, pressure sensors have achieved substantial advancement in performance utilising smart structural designs, nanostructures and advanced materials, nanostructures.

In this report, we introduce and demonstrate a new principle that significantly enhances the sensitivity of a micromachined pressure sensor.

RESULTS

Table 1 shows parameters of the pressure sensors such as diaphragm, the material types, doping concentration and thickness of silicon carbide nanofilms grown on silicon and of the diaphragm. For example, single crystalline heavily doped 3C-SiC with thickness of 300 nm was grown on a p-type Si substrate (100) by low pressure chemical deposition (LPCVD) method at a temperature of 1000 °C.

Table 1: Parameters of the pressure sensor

Parameter	Values	
Diaphragm	5 mm x 5 mm	
Materials	Top layer	3C-SiC
	Substrate	Si
Thickness	3C-SiC	300 nm
	Diaphragm	225 µm
Doped concentration	3C-SiC	$5 \cdot 10^{18}$ cm^{-3}
	Si	$5 \cdot 10^{14}$ cm^{-3}

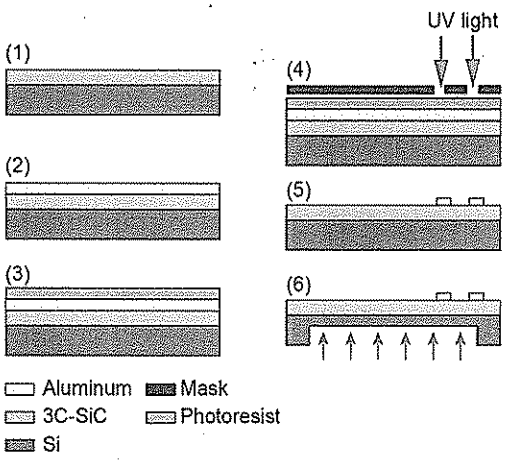

Figure 1: Fabrication process

Figures 2 and 3 show repeatability of the fractional change of output voltage as air pressure of 60 kPa was periodically turned ON and OFF under dark and light conditions, respectively. It can be seen that by controlling simultaneously light illumination and electric field in the 3C-SiC layer, the relative change of the resistance under light illumination was at least five orders of magnitude higher than that in dark condition. Figure 4 shows the sensitivity of the pressure sensor under both dark and light conditions. The sensitivity of the pressure sensor was enhanced approximately 185,100 times reaching a sensitivity of 0.87 kPa^{-1}, which is much higher than semiconductor-based machined pressure sensors.

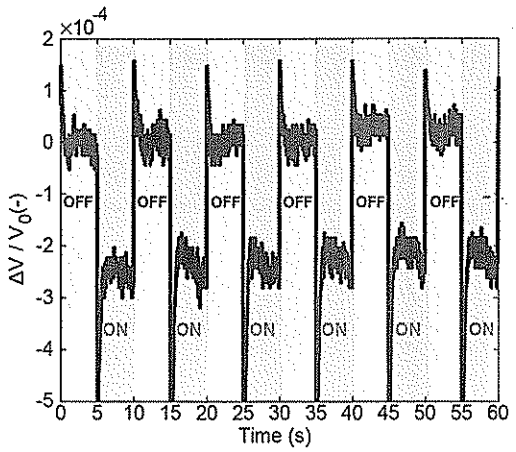

*Figure 2: The repeatability of the fractional change in voltage under **dark** condition as the pressure of 60 kPa was periodically turned ON and OFF*

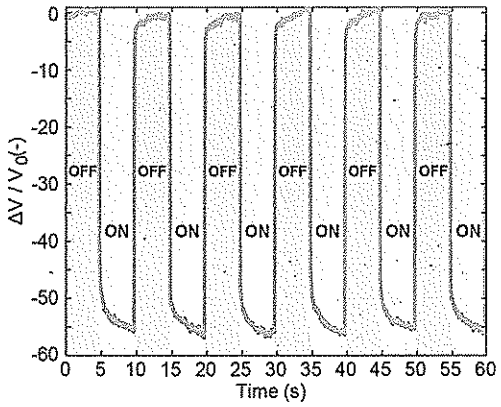

*Figure 3: The repeatability of the fractional change in voltage under **light** condition as the pressure of 60 kPa was periodically turned ON and OFF*

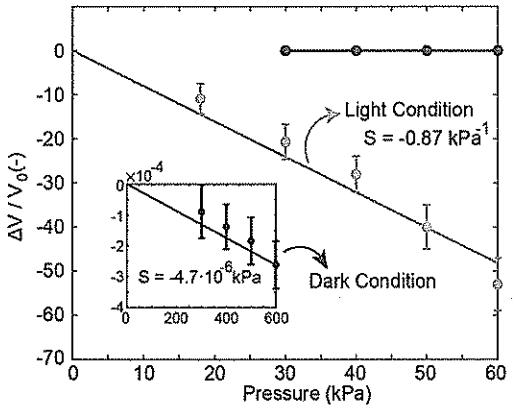

Figure 4: The sensitivity of the pressure sensor

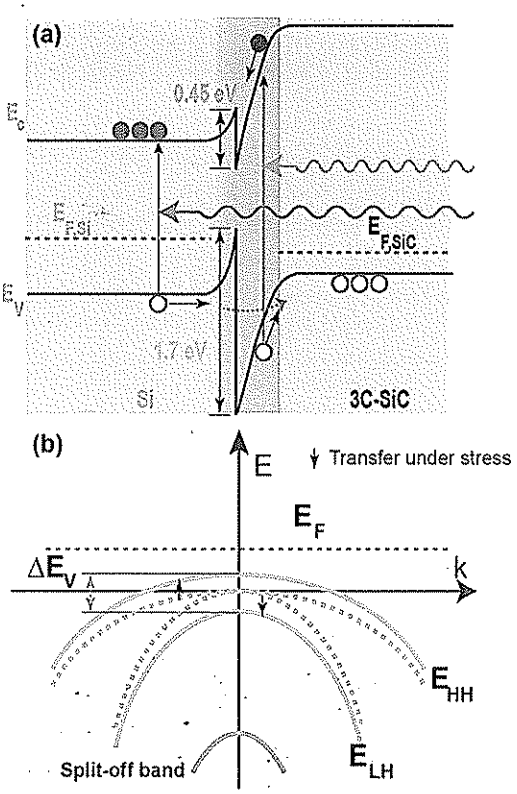

Figure 5: (a) Band energy and (b) E-k characteristic in 3C-Si thin film.

REFERENCES

1. Nguyen, T.-K., et al., *Highly sensitive 4H-SiC pressure sensor at cryogenic and elevated temperatures.* Materials & Design, 2018. **156**: p. 441-445.
2. Pan, L., et al., *An ultra-sensitive resistive pressure sensor based on hollow-sphere microstructure induced elasticity in conducting polymer film.* Nature communications, 2014. **5**: p. 3002.
3. Schwartz, G., et al., *Flexible polymer transistors with high pressure sensitivity for application in electronic skin and health monitoring.* Nature communications, 2013. **4**: p. 1859.
4. Barlian, A.A., et al., *Review: Semiconductor Piezoresistance for Microsystems.* Proc IEEE Inst Electr Electron Eng, 2009. **97**(3): p. 513-552.
5. Xu, F., et al., *High-sensitivity Fabry–Perot interferometric pressure sensor based on a nanothick silver diaphragm.* Optics letters, 2012. **37**(2): p. 133-135.
6. Hu, Y., et al., *Triboelectric nanogenerator built on suspended 3D spiral structure as vibration and positioning sensor and wave energy harvester.* ACS nano, 2013. **7**(11): p. 10424-10432.

INFLUENCES OF THE TEMPERATURE AND HUMIDITY ON QUALITY FACTORS OF MEMS BRIDGE RESONATORS IN AIR ENVIRONEMTNS

Chi Cuong Nguyen[1,*], Trinh Xuan Thang[1], Tran Duy Hoai[1], Nguyen Thanh Phuong[1], Vu Le Thanh Long[1], Truong Huu Ly[1], Hoang Ba Cuong[1], Le Quoc Cuong[2], Ngo Vo Ke Thanh[1]
[1]The Research Laboratories of Saigon High-Tech-Park, Saigon Hi-Tech Park Lot I3, N2 Street, Saigon Hi-Tech-Park, District 9, Ho Chi Minh city, Vietnam;
[2] Institute for Computational Science and Technology, SBI Building, Quang Trung Software City, Tan Chanh Hiep Ward, District 12, Ho Chi Minh city, Vietnam.
*Email: cuong.nguyenchi@shtplabs.org

In this paper, the modified molecular gas lubrication (MMGL) equation is used to solve for the squeeze film damping (SFD) on dynamic performance of MEMS bridge resonators. The effective viscosity of moist air is used to modify the MMGL equation to consider the effects of temperature and relative humidity in gas rarefaction. Internal structural damping (Thermoelastic damping (TED) and anchor loss), which are the other dominant damping mechanisms of MEMS bridge resonators, is also taken into account. Thus, the influences of temperature and relative humidity are discussed on the *Q*-factors of MEMS bridge resonators in wide range of gas rarefaction (pressure, *p* and accommodation coefficients, ACs) and resonant mode of vibration.

Key words: Quality factor, MEMS bridge resonators, relative humidity, temperature, gas rarefaction

INTRODUCTION

Background

In MEMS resonators, the most important dynamic characteristics of quality factor (*Q*-factor). Physically, the *Q*-factor is defined as a ratio of rate of energy loss and stored energy of resonators. Higher *Q*-factor (lower energy loss), which is one of crucial requirement of MEMS resonators operated in higher sensitivity, and long-term stability of sensing systems.

In MEMS bridge resonators, there have been several damping mechanisms of oscillating structures that minimized the *Q*-factor of MEMS resonators. The external squeeze film damping (SFD), which is a dominant damping source appeared as the gas flow squeezed in small gas film spacing [1]. The internal structure damping sources such as the thermoelastic damping (TED) (loss into the structure) [2] and support loss (loss into the substrate) [3] are the other dominant damping mechanisms.

In gas rarefaction conditions, the effective viscosity of moist air, which changes significantly as functions of temperature and relative humidity in gas rarefaction, influences on the performance of MEMS resonators in gas rarefaction [4-8]. To improve the *Q*-factor of resonators due to the SFD, Therefore, the influences of temperature and relative humidity in wide range of gas rarefaction of air ambient environment must be carefully considered to improve the *Q*-factor of resonators.

RESULTS

In Fig.1(*a*), quality factor (Q_{SFD}) of dry air (*RH*=0%) increases slightly as *T* increases, whereas Q_{SFD} of moist air decreases significantly as temperature (*T*) and relative humidity (*RH*) increases at higher gas rarefaction (p_a=100 Pa). While, in Fig.1(*b*), Q_{SFD} decreases significantly and then increases slightly as *T* and *RH* increase at lower gas rarefaction (p_a=100,000 Pa). Thus, the obtained results can be useful to explain the influences of temperature and relative humidity on the total quality factor (Q_T) of MEMS cantilever resonator in wide range of gas rarefaction (p_a, ACs) and resonant mode of vibration conditions.

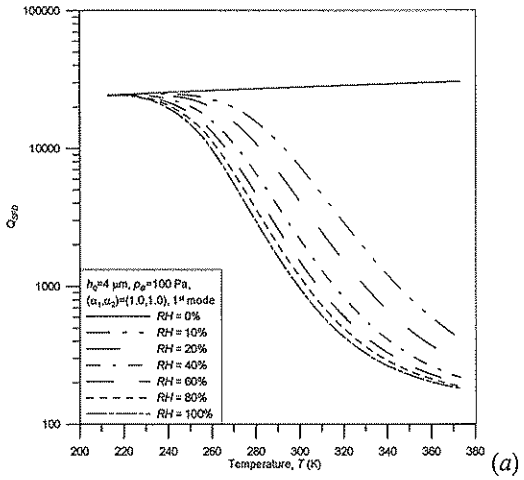

(*a*)

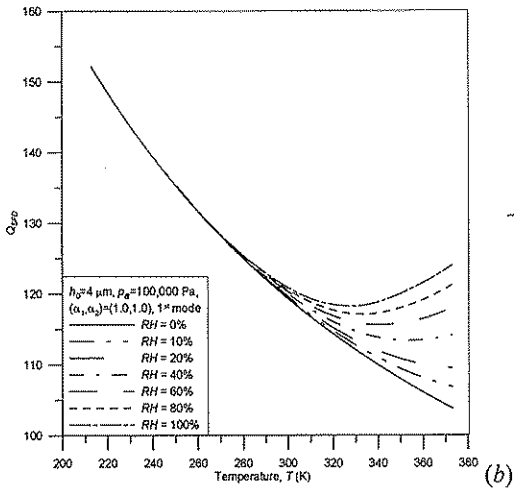

Figure 1: Quality factor of SFD (Q_{SFD}) at higher gas rarefaction (p_a=100 Pa), (c) at lower gas rarefaction (p_a=100,000 Pa) versus ambient temperature (T) for different relative humidity (RH).

CONCLUSION

The results showed that the Q-factor of SFD of moist air decreases more significantly as temperature and relative humidity increase at higher gas rarefaction (lower p, and ACs), while, Q-factor decreases and then increases slightly with temperature and then increases as temperature and relative humidity increases at lower gas rarefaction (higher p, and ACs). Influence of relative humidity and temperature on total Q-factors of MEMS bridge resonators becomes more significantly in higher gas rarefaction (lower p and ACs), and lower mode of vibration conditions.

ACKNOWLEDGEMENTS

This research was supported by the annual projects of The Reasearch Labortories of Saigon High Tech Park in 2019 according to decision No. 102/QĐ - KCNC of Management Board of Saigon High Tech Park and contract No. 01/2019/HĐNVTX-KCNC-TTRD (Project number 3).

REFERENCES

[1] H. Hosaka, K. Itao, S. Kuroda, "Damping characteristics of beam-shaped micro-oscillators", *Sensor. Actuat. A-Phys.*, vol. 49, pp. 87–95, 1995.

[2] H. Zhou, P. Li, W. Zuo, "Thermoelastic damping in micro-wedged cantilever resonator with rectangular cross-section", in *2016 IEEE International Conference on Mechatronics and Automation*, 2016, pp. 1590-1595.

[3] M. Jandak, T. Neuzil, M. Schneider, U. Schmid, "Investigation on different damping mechanisms on the Q factor of MEMS resonators", *Procedia Engineering*, vol. 168, pp. 929-932, 2016.

[4] E. Hosseinian, P.-O. Theillet, O.N. Pierron, "Temperature and humidity effects on the quality factor of a silicon lateral rotary micro-resonator in atmospheric air", *Sensor. Actuat. A-Phys.* vol. 189, pp. 380–389, 2013.

[5] C. C. Nguyen, W. L. Li, "Effect of gas rarefaction on the quality factors of micro-beam resonators", *Microsyst. Technol.* vol. 23, pp. 3185–3199, 2017.

[6] C. C. Nguyen, W. L. Li, "Effects of surface roughness and gas rarefaction on the quality factor of micro-beam resonators", *Microsyst. Technol.* vol. 23, pp. 3489–3504, 2017.

[7] C. C. Nguyen, W. L. Li, "Influences of temperature on the quality factors of micro-beam resonators in gas rarefaction", *Sensor. Actuat. A-Phys.*, vol. 261 pp. 151–165, 2017.

[8] C. C. Nguyen, V. K. T. Ngo, H. Q. Le, W. L. Li, "Influences of relative humidity on the quality factors of MEMS cantilever resonators in gas rarefaction", *Microsyst. Technol.* vol. 25, pp. 2767–2782, 2018.

A LABEL-FREE DNA SENSOR BASED ON A MICROCANTILEVER PLATFORM

Quang Thinh Tran, Thi Thuong Trinh and Anh Tuan Mai

Microfabrication Laboratory at Hoa Lac Hightech Park
National Center for Technological Progress, C6 Thanh Xuan Bac, Thanh Xuan, Hanoi
*Email: thinh.tran@mph.vn

In this work, we report the application of microcantilevers for the development of highly sensitive label-free sensors in DNA detection. The operation of microcantilever-based DNA sensors is achieved from a combination of the traditional DNA hybridization approach and the nano-mechanical analysis. The change of nano-mechanical vibrations, caused by DNA hybridization on the microcantilever surface, were recognized by using the optical lever method with the Scanning Laser Analyzer (SCALA). This approach is considered as a nondestructive testing technique for the effective DNA detection.

Key words: Microcantilever; label-free detection of DNA; nano-mechanics

THE PROSPECTIVE OF THE INTERNET OF ENERGY

Duy-Dinh Nguyen[1,*], Nguyen Gia Minh Thao[2], Huynh-Ngoc Tran[2], Kazuto Yukita[1]
[1]Aichi Institute of Technology; [2]Toyota Technological Institute
*Email: nguyenduydinh@aitech.ac.jp

In the recent years, the power system encounters a massive conversion from centralized generation into dispersed generation. A dispersed system includes of many micro-grids, storage devices, renewable energy resources interconnected to supply electric power. In the such system, the need of a novel electricity trading paradigm results in a new market model, new roles of players, new measurement equipment and techniques, etc. and finally yield to the so-called Internet of Energy. This paper introduces such the power system paradigm from the device and instrument aspects.

Key words: Internet-of-Energy, dispersed generation, renewable energy, energy meter, electricity trading

INTRODUCTION

In the recent years, dispersed or distributed generation attracts not only the power system operators and the policy makers but also many other sections of the industry [1]. Moreover, since the fossil-fuel resources are likely going to be exhausted and the environmental conservation is a crucial issue, the use of renewable energy sources is presently a salient advance and becomes more popular in many countries. Photovoltaic (PV) and wind power systems with prominent features such as an unlimited power and environmentally friendly resource are playing an ever-increasingly major role in supplying electricity. For example, renewable energy has been one of the quickest-growing energy sources in the United States (US) in recent fifteen years, which was around 15% of the US's electricity generation in 2016. Besides, in the European Union (EU), wind energy was 12% and 14% of the EU's electricity in 2017 and 2018, respectively. In addition, PV solar power systems installed in the EU was 9.2 GW and 11.0 GW in 2017 and 2018, respectively; the increase is around 20%.

To achieve good efficiency in operating a real PV or wind energy system, two main factors should be considered thoroughly. The first one is impacts of weather parameters; the other is effects of power converters, controllers, energy storage system and loads utilized in the PV/wind system. Obviously, the weather condition is out of the user's control and often alters suddenly. Moreover, since characteristics of PV array and wind turbine are highly affected by weather parameters and the electric grid is nonlinear object, advanced design and topologies of power-electronic converters and intelligent control methods are appropriate and useful to substantially improve the overall efficiency of renewable energy systems.

As various kinds of energy resources tend to interconnect to each other, such as PV, wind power, AC grid, DC storage, HVDC, etc., the need of a new power system paradigm has been arisen and excites all aspects of the industry. First, new devices called Solid-State-Transformers (SST) [2] emerge to help interconnecting the grid. An SST provides galvanic isolation, compact and high efficiency, high power density. Furthermore, it has many interesting advantages which absent in the case of line frequency transformers such as asynchronous interconnection, DC/AC, DC/DC or AC/DC power conversion, communication capability, etc. In particular, the communication capability makes the SSTs smart to become key enabler of the Internet of Energy (IoE).

The IoE paradigm was first introduced about ten years ago [3]. When each home has its own power generation such as PV or battery, the IoE allows them to sell the excessive energy back to the electric grid. Therefore, in the IoE, the energy sellers/buyers are not discriminated but defined the same as prosumers; the distributed grid now becomes the energy shipper; the traditional hierarchical energy trading model is now turned into peer-to-peer transaction and the energy selling/buying contract between user and the electricity companies is now becoming a shipping contract [4]. Such the paradigm is very promising as it has been deployed and testing in the US and many European countries such as the UK, Germany, etc.

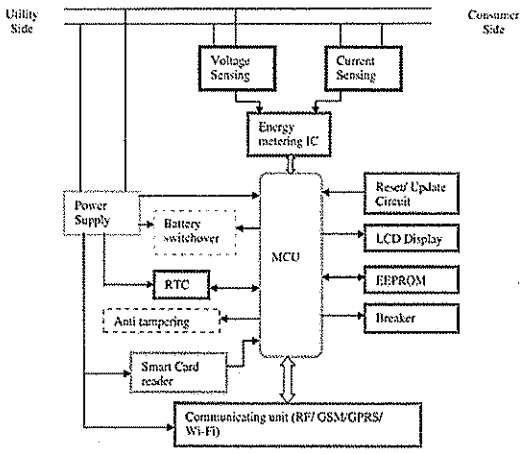

Fig. 1. Typical structure of a modern smart meter [5].

Beyond the energy conversion, the IoE operation is based on "data". The data is usually not measured by using the conventional mechanical meters but the smart meters. Fig. 1 describes the typical hardware configuration of a modern smart meter. The most important component here is the energy metering integrated circuit (IC) which is in charge of calculating the consumption energy of user from the measured voltages and currents. Some kinds of metering IC allow to calculate the energy in both directions. After that, a micro-controller unit (MCU) processes the obtained information and then displays, stores and/or sends to the communication bus (e.g. Wifi, GSM, 4G, etc.).

As SSTs are introduced, the smart meters can be integrated onto the SST. An SST measures the electrical information such as voltages, currents, frequency, phase for control and protection purposes. Based on the real time measurement, other information like consumption energy, active and reactive powers, power quality, etc. can be also calculated. Moreover, the SST is controlled by a micro-computer (such as DSP, ARM, etc.) which is usually much more powerful than an MCU. The micro-computer can also communicate to other micro-computer-based SSTs to enable the IoE.

It can be seen that, all components shown in Fig. 1 are also available in a much more complex SST control and management system. For example, the conceptual power system proposed by the future renewable electric energy delivery and management (FREEDM) center depicted in Fig. 2 consists of several SSTs interconnected via a 12 kV bus. Each SST has an intelligent energy management (IEM) system. All the IEM are supervised by a distributed grid intelligence (DGI) system via wireless communication. Obviously, the smart meter can be integrated directly into such system. Therefore, the need of a standalone energy meter can be eliminated.

As all the collected data can be transmitted wirelessly by the micro-computer via the Internet, other Internet services and applications can be also applied. For example, cloud computing can be employed to reduce the computation burden of the micro-computer; big data and block-chain technology can be also deployed to manage the data and to facilitate the trading process with the Energy Coins [6]; all the transactions can now be undertaken automatically and paperlessly in the real time via mobile apps instead of monthly by cash.

CONCLUSION

This paper has briefly introduced a new power system paradigm. It is suitable for the distributed power generation where each micro-generation can become either a producer or consumer. A communication network can be formed between the "*pro-sumers*" which is defined as the Internet of Energy. The key enabler of such the paradigm is the SST. An SST includes of power electronics converter, energy meter unit and communication unit.

In the last ten years, more and more projects upon this idea are kicked-off and now underlying testing process in the US and many European countries. This implies that the IoE paradigm is a very promising model that can revolutionize the use and trading of energy in the near future.

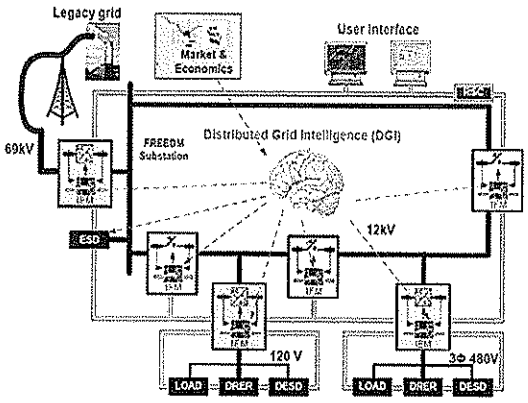

Fig. 2. The conceptual FREEDM electric grid [3]

REFERENCES

[1] Lopes JP, Hatziargyriou N, Mutale J, Djapic P, Jenkins N. Integrating distributed generation into electric power systems: A review of drivers, challenges and opportunities. Electric power systems research. 2007 Jul 1;77(9):1189-203.

[2] She X, Huang AQ, Burgos R. Review of solid-state transformer technologies and their application in power distribution systems. IEEE journal of emerging and selected topics in power electronics. 2013 Aug 15;1(3):186-98.

[3] Huang AQ, Crow ML, Heydt GT, Zheng JP, Dale SJ. The future renewable electric energy delivery and management (FREEDM) system: the energy internet. Proceedings of the IEEE. 2010 Nov 11;99(1):133-48.

[4] Sousa T, Soares T, Pinson P, Moret F, Baroche T, Sorin E. Peer-to-peer and community-based markets: A comprehensive review. Renewable and Sustainable Energy Reviews. 2019 Apr 1;104:367-78.

[5] Weranga KS, Kumarawadu S, Chandima DP. Smart metering design and applications. Singapore: Springer; 2014.

[6] Wang N, Zhou X, Lu X, Guan Z, Wu L, Du X, Guizani M. When energy trading meets blockchain in electrical power system: The state of the art. Applied Sciences. 2019 Jan;9(8):1561.

Local Control of Molecular Nanochemical Reactions*

Masakazu Aono
Fellow & Executive Advisor
International Center for Materials Nanoarchitectonics (MANA),
National Institute for Materials Science (NIMS), Tsukuba, Japan.

Two topics ① "Formation of conductive polymer chains at designated local positions" and ② "Reversible control of C_{60}-C_{60} bound and unbound states at designated local positions" are discussed. These interesting phenomena were already reported by us several years ago, but in the present paper the underlying mechanisms of the phenomena are discussed in detail. Also, our recent efforts to practically (industrially) use the phenomena are reported.

① Formation of Conductive Polymer Chains at Designated Local Positions

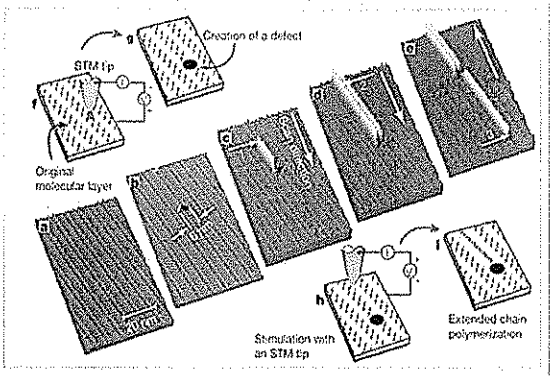

② Reversible Control of C_{60} - C_{60} Bound and Unbound States at Designated Local Positions

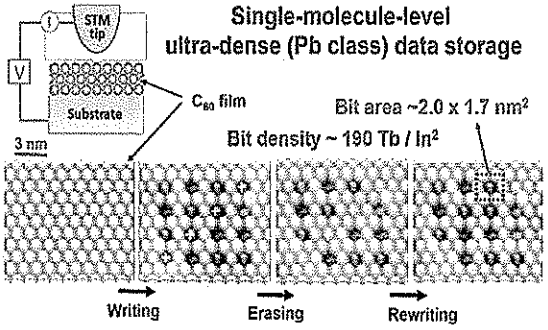

*In collaboration with Yuji Okawa and Tomonobu Nakayama, MANA/NIMS.

SILOXANE POLYURETHANE NANO COMPOSITES FOR BIOMEDICAL APPLICATIONS

Raju Adhikari[1], Nuha Y. Al-Attabi[1,2], Mark Bown[1], Peter Cass[1], Meg Evans[3], Pathiraja Gunatillake[1], Gagan Kaur[1], Francois Malherbe[2], and Aimin Yu[21]

[1]CSIRO Manufacturing, Bayview Avenue, Clayton, VIC 3168, Australia
[2] Faculty of Science Engineering and Technology, Swinburne University of Technology, Hawthorn 3122, Australia

[3]CSIRO Manufacturing, Julius Avenue, North Ryde, NSW 2113, Australia

Silicone-rich polyurethanes and polyurethaneureas[1] have attracted significant interest in the development of long-term implantable medical devices[2] on account of their proven biocompatibility and long-term biostability. Their resistance to calcification, excellent haemocompatibility, and creep resistance have made possible the development of durable pacemaker leads (Optim™, Tendril™, St Jude), and more recently all-polymer heart valves (LifePolymer™, Tria™ valve, Foldax).

Electrically conductive polymers have attracted considerable interest from researchers in the development of biomedical devices including biosensors and biomedical implants such as probes for deep brain stimulation and bionic eyes. Many of the inherently conducting polymers such as polyaniline and polyacetylene lack the processability required to lend themselves useful in the fabrication of devices.

Nano composite materials comprised of conducting particles in a flexible biostable, biocompatible polymer matrix hold some attraction in this space IF they can be formulated to achieve good conductivity whilst still maintaining their inherent properties.

We report here a study on the synthesis and characterization of a series of conducting siloxane-rich polyurethane [Elast-Eon™ (E2A), Aortech Biomaterials] nano composites formulated using a range of conducting nano particulate materials including combinations of gold nanoparticles[2], graphene[3], and silver nano wires. The composites were evaluated for their electrical conductivity, mechanical properties, thermal stability, and cell viability.

1. Gunatillake, Pathiraja A.; Dandeniyage, Loshini S.; Adhikari, Raju; Bown, Mark; Shanks, Robert; Adhikari, Benu, *Polymer Reviews* (2019), 59(3), 391-417;
2. Kaur, Gagan; Adhikari, Raju; Cass, Peter; Bown, Mark; Gunatillake, Pathiraja, *RSC Advances* (2015), 5(47), 37553-37567;
3. Al-Attabi, Nuha Y.; Kaur, Gagan; Adhikari, Raju; Cass, Peter; Bown, Mark; Evans, Meg; Gunatillake, Pathiraja; Malherbe, Francois; Yu, Aimin, *Journal of Materials Science* (2017), 52(19), 11774-11784;
4. Kaur, Gagan; Adhikari, Raju; Cass, Peter; Bown, Mark; Evans, Margaret D. M.; Vashi, Aditya V.; Gunatillake, Pathiraja, *RSC Advances* (2015), 5(120), 98762-98772;
5. Al-Attabi, Nuha Y.; Adhikari, Raju; Cass, Peter; Bown, Mark; Gunatillake, Pathiraja A.; Malherbe, François; Aimin Yu, *Materials Science and Technology* (2019), 35(4), 462-468.

SINGLE-CRYSTAL TO SINGLE-CRYSTAL TRANSFORMATIONS IN IRON(III) SPIN CROSSOVER COMPLEXES

M. Muadtrap,[a] K. S. Murray,[b] W. Phonsri,[b] J. K. Clegg,[c] P. Harding[a] and D. J. Harding*[a]
[a] *FuNTech Center of Excellence, Walailak University, Nakhon Si Thammarat, Thailand.* [b] *School of Chemistry, Monash University, Melbourne, Victoria, Australia.* [c] *School of Chemistry and Molecular Biosciences, The University of Queensland. St. Lucia. Queensland, Australia.*
*Email: hdavid@mail.wu.ac.th

Molecular switches are of great interest for use in a range of future technologies. Spin crossover (SCO) complexes are amongst the best studied of molecular switches as the compounds are easy to prepare and can operate at room temperature.[1] While most SCO complexes are of Fe(II),[2] more recently Fe(III) compounds have been shown to be robust and exhibit strongly cooperative SCO.[3–6] In this work we report the synthesis of two new complexes, $[Fe(qsal\text{-}X)_2]MeSO_3 \cdot MeOH$ (X = Br, I) which exhibit gradual and abrupt SCO, respectively. Heating results in a single-crystal to single-crystal transformation to give the desolvated complexes. Detailed structural investigations of the MeOH solvates and $[Fe(qsal\text{-}X)_2]MeSO_3$ show subtle changes in the packing that impact both $T_{1/2}$ and the abruptness of the spin transition.

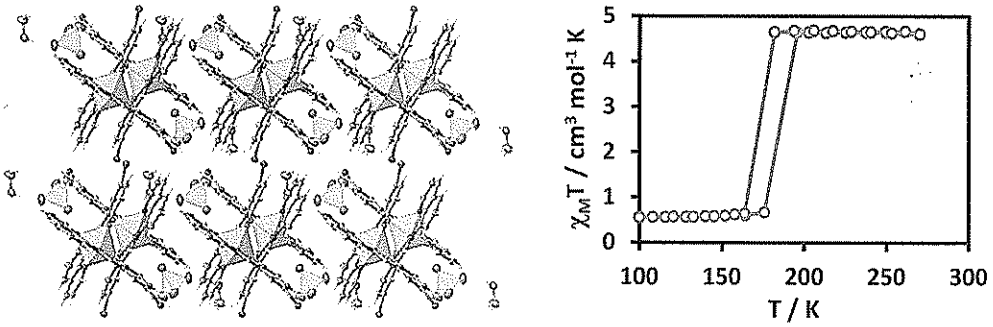

Figure 1. View of the packing in $[Fe(qsal\text{-}I)_2]MeSO_3 \cdot MeOH$ at 150 K and the SQUID profile.

References

1 *Spin-Crossover Materials: Properties and Applications*; Halcrow, M. A., Ed.; John Wiley & Sons, Ltd: Chichester, 2013.
2 Gütlich, P.; Gaspar, A. B.; Garcia, Y. Spin State Switching in Iron Coordination Compounds. *Beilstein J. Org. Chem.* **2013**, *9*, 342–391.
3 Harding, D. J.; Harding, P.; Phonsri, W. Spin Crossover in Iron(III) Complexes. *Coord. Chem. Rev.* **2016**, *313*, 38–61.
4 Bertoni, R.; Lorenc, M.; Tissot, A.; Boillot, M. L.; Collet, E. Femtosecond Photoswitching Dynamics and Microsecond Thermal Conversion Driven by Laser Heating in FeIII Spin-Crossover Solids. *Coord. Chem. Rev.* **2015**, *282–283*, 66–76.
5 Phonsri, W.; Harding, P.; Liu, L.; Telfer, S. G.; Murray, K. S.; Moubaraki, B.; Ross, T. M.; Jameson, G. N. L.; Harding, D. J. Solvent Modified Spin Crossover in an Iron(III) Complex: Phase Changes and an Exceptionally Wide Hysteresis. *Chem. Sci.* **2017**, *8*, 3949–3959.

We thank the Thailand Research Fund (BRG6180008) for funding this research.

MULTIMODAL SWITCHING OF RESORCINARENE NANOMOLECULES

Jonathan P. Hill[1,*], Daniel T. Payne[1]
[1]International Center for Materials Nanoarchitectonics, National Institute for Materials Science, Namiki 1-1, Tsukuba, Ibaraki 305-0044, Japan
*Email: Jonathan.Hill@nims.go.jp

The introduction of anti-oxidant phenol groups to organic chromophore structures significantly affects their properties. We demonstrate this here by establishing an organic molecular switching manifold with multimodality of operation based on the development of a substituted resorcinarene macrocycle. Intramolecular charge-transfer states, involving hemiquinhydrones are probed and these interactions are used to construct an oxidation-state-coupled molecular switching manifold that reports its switch-state conformation *via* striking variation in its electronic absorption spectra. The coupling of two different oxidation states with two different charge-transfer states within one macrocyclic scaffold delivers up to five different optical outputs. This molecular switching manifold exploits intramolecular coupling of multiple redox active substituents within a single molecule.

Key words: resorcinarene, molecular switch

INTRODUCTION

Background

Molecules that can exist in multiple states with the possibility of toggling between those states based on different stimuli have potential for use in molecular switching or sensing applications. Resorcinarene macrocycles are widely studied because they tend to self-assemble as nanocapsular structures when isolated in the appropriate isomeric form. That work has been facilitated by the availability of the macrocycle in large quantities from high-yielding one-pot multi-gram reactions. While host-guest interactions have been widely studied for these systems, we felt that the essential chemistry of the resorcinarenes had more to offer based on the introduction of functionality beyond simple aryl or alkyl substituents, and so we commenced our study by applying a common research theme in our laboratories: introduction of redox-active moieties to chromophore molecules. Hence, we introduced phenolic substituents (2,6-di-t-butylphenol, butylated-hydroxytoluene (BHT) groups), which are capable of existing in phenolic, quinonoid and even radical states.[1] To date, we have exploited these substituents mostly in the context of simple porphyrin molecules with a focus on sensing applications.[2,3]

RESULTS

Multimodal chemical or photochemical oxidative switching of an antioxidant-substituted resorcinarene macrocycle is reported.[4] Resorcinarene meso-substituted with BHT groups was prepared and we were subsequently excited to discover that it could indeed be isolated in three different oxidation states. Most importantly, oxidation steps can be performed independently either by exposure to light or chemically. Actually, photochemically induced oxidation had caused difficulties in the identification of the compounds even with all compounds being X-ray crystallographically characterized. While the forward oxidation steps proved reversible, it was not until we observed the compounds under acidic conditions that the final piece of the puzzle for our switching manifold fell into place. Higher oxidation states of the molecule exhibit intense colors in the presence of acids in solution and solid states. These states could also be accessed by performing oxidation steps under acidic conditions. The whole process, related electronic absorption spectra and the colours of the different switching nodes are shown in Figure 1.

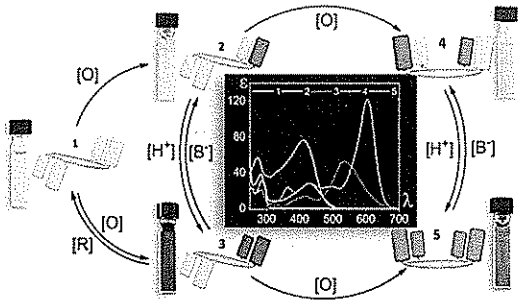

Figure 1. Stable states of the resorcinarene molecular switch. 1: starting state (neutral, not oxidized), 2: mono-oxidized (mono-quinonoid), 4: doubly oxidized (bis-quinonoid). 3 and 5 are the acid stabilized charge transfer states of 2 and 4, respectively. Central panel shows the electronic absorption spectra of each state.

We could eventually assign the intensely colored species as intramolecular charge transfer (C-T) states whose formation is promoted by protonation of quinonoid oxygen atoms. These C-T states are thought

also to be stabilized by hydrogen bonding involving the acidic reagent. Different oxidation states of the manifold could be X-ray crystallographically studied revealing that conformational switching also occurs (Figure 2).

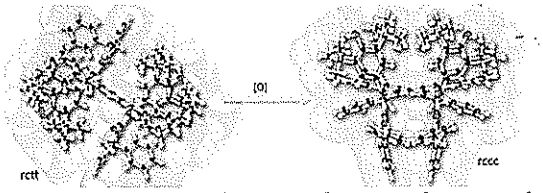

Figure 2. Conformational switching of resorcinarenes.

CONCLUSION

This molecular switching work illustrates that there are other aspects of the resorcinarene macrocycles that deserve further investigation.[5] These are complementary to the already fantastic array of supramolecular systems that have been reported for the resorcinarenes. We also expect that synergies will come about between the existing nanocapsular research area and emerging properties of this important class of macrocycle.

ACKNOWLEDGEMENTS

This work was partly supported by World Premier International Research Center Initiative (WPI Initiative), MEXT, Japan. The authors are grateful to Japan Society for the Promotion of Science (JSPS) for a JSPS Fellowship (to D.T.P.). This work was also partially supported by JSPS KAKENHI (Coordination Asymmetry) (Grant No. JP16H06518), and CREST, JST (Grant No. JPMJCR1665).

REFERENCES

[1] S. Ishihara, J. P. Hill, A. Shundo, K. Ohkubo, S. Fukuzumi, M. R. J. Elsegood, S. J. Teat, K. Ariga "Reversible Photoredox Switching of Porphyrin-bridged Bis-2,6-di-*t*-Butyl Phenols" *J. Am. Chem. Soc.*, vol 133, 16119–16126, 2011

[2] J. Labuta, J. P. Hill, S. Ishihara, L. Hanykova, K. Ariga, "Chiral Sensing using Non-chiral Porphyrins", *Acc. Chem. Res.*, vol. 48, pp. 521-529, 2015. 48, 521–529, 2015

[3] J. P. Hill, N. K. Subbaiyan, F. D'Souza, Y. Xie, S. Sahu, N. M. Sanchez-Ballester, K. Ariga, "Antioxidant-substituted Tetrapyrazinoporphyr-azine as Fluorescent Sensor for Basic Anions", *Chem. Commun.* vol 48, 3951–3953, 2012.

[4] D. T. Payne, W. A. Webre, Y. Matsushita, N. Zhu, Z. Futera, J. Labuta, W. Jevasuwan, N. Fukata, J. S. Fossey, F. D'Souza, K. Ariga, W. Schmitt, J. P. Hill, "Multimodal Switching of a Redox-active Macrocycle", *Nat. Commun.* vol 10, 1007, 2019.

[5] D. T. Payne, J. P. Hill, "Emerging Aspects of Resorcinarene Chemistry", submitted.

RECENT DEVELOPMENTS IN 1,8-NAPHTHALIMIDE CHEMISTRY: IMPROVED METHODOLOGY AND NEW APPLICATIONS

F. Pfeffer, T. Ashton, C. Fleming, K. Hearn and E. Rudebeck
School of Life and Environmental Sciences, Faculty of Science and Technology, Deakin University, Waurn Ponds, 3217, Australia.

*Email: fred.pfeffer@deakin.edu.au

Naphthalimides have proven themselves to be one of the most robust and widely used fluorophores available to chemists worldwide. As such new or improved methods to introduce functionality to these luminophores can further enhance their utility and also the suite of possible applications.

In this talk Improvements in methods for accessing a range of both 3 and 4 substituted naphthalimides will be presented.[1,2] The suite of functional groups being appended include hydroxy, alkoxy, amino, amido, ureido and carbamato.

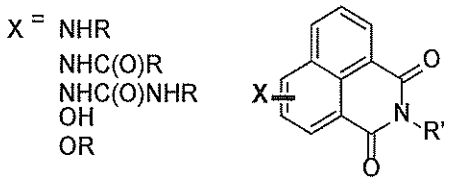

The use of this methodology in the development of new highly fluorescent, highly selective, histone deacetlyase inhibitors (HDACi) will also be presented along with details of their use in cellular and in-vivo imaging.[3]

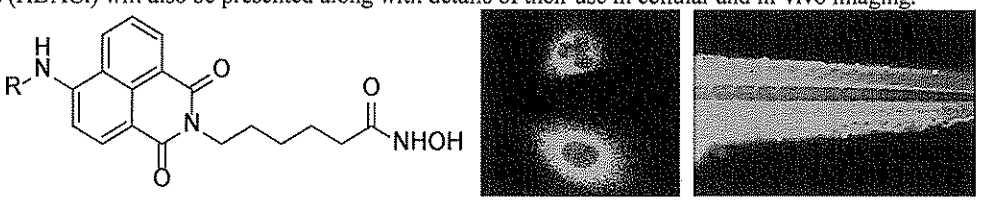

References

[1] Fleming, C.L., Nalder, T.D., Doeven, E.H., Pfeffer, F.M., Ashton, T.D., et Al, **2016**, *Dyes and Pigments*, 126, 118-120.

[2] Hearn, K.N., Nalder, T.D., Cox, R.P., Pfeffer, F.M., Ashton, T.D. *et Al*, **2017**, *Chemical Communications* 53(91), 12298-12301.

[3] Fleming, C.L., Natoli, A., Schreuders, J., Ashton, T.D., Pfeffer, F.M. *et Al*, **2019**, *European Journal of Medicinal Chemistry*, 321-333.

DIVERSE PROPERTIES OF PORPHYRIN DERIVATIVES

Jan Labuta*
International Center for Materials Nanoarchitectonics (WPI-MANA),
National Institute for Materials Science (NIMS), Tsukuba, Japan
*Email: Labuta.Jan@nims.go.jp

Porphyrins are functional dyes that play essential role in living organisms. By means of synthetic modifications of porphyrin macrocycle we have demonstrated broad range of properties and applications of these derivatives, such as: chirality[1-3], pH[4,5], anions or impurity[6] sensing, phase separation and also their interesting non-trivial intra-molecular dynamic behaviour[7]. The physicochemical aspects together with several potential applications of these porphyrin derivatives will be shown.

Key words: porphyrin, chirality, pH, impurity, phase separation, molecular dynamics

INTRODUCTION

Background

Porphine and its derivatives (i.e. the porphyrins, Fig. 1) are functional pigments that can complex a great variety of metal cations. In biological systems, porphyrins play essential roles as photosynthetic antenna and reaction centre components, in the heme proteins. The large extinction coefficients of porphyrin chromophores imply photo-electronic applications. In addition, numerous synthetic procedures are available for their future modifications permitting a continuous expansion of the family of porphyrin compounds.

RESULTS AND CONCLUSION

In this paper, we present: 1) Chirality sensing using porphyrins,[1-3] and its potential use for 3D magnetic resonance imaging (MRI) of chirality in living samples, 2) Phase separation (and pH response) of water soluble temperature sensitive porphyrins, and 3) Intra-molecular dynamics including tautomerism and macrocycle inversion[7] of oxidized porphyrin derivative.

These effects (Fig. 1) are only weakly connected, which emphasizes the diverse utilizations of porphyrin as a basic building block for applications in various fields, such as molecular sensors, switches, MRI contrast agents and/or PDT sensitizing agents.

In summary, the design of novel multi-responsive porphyrin derivatives can combine above mentioned attractive features for targeted applications, such as, photodynamic therapy (PDT), 3D magnetic resonance imaging (MRI) of chirality, or establishment of pH scales in organic solvents.

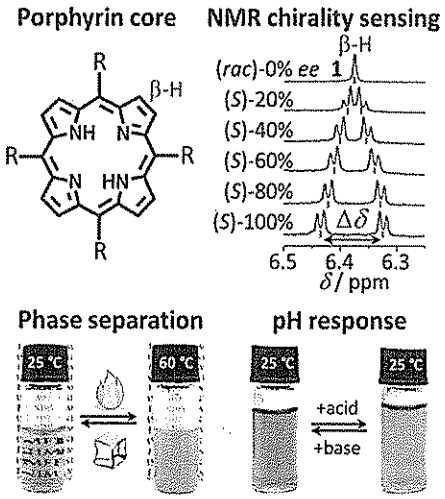

Figure 1: Porphyrin core, a basic building block. Chirality, temperature (phase separation) and pH responses are shown.

REFERENCES

[1] J. Labuta, J. P. Hill, S. Ishihara, L. Hanyková, K. Ariga, "Chiral Sensing by Nonchiral Tetrapyrroles", *Acc. Chem. Res.*, *48*, 521, 2015.

[2] J. Labuta, S. Ishihara, T. Šikorský, Z. Futera, A. Shundo, L. Hanyková, J. V. Burda, K. Ariga and J. P. Hill, "NMR Spectroscopic Detection of Chirality and Enantiopurity in Referenced Systems without Formation of Diastereomers", *Nat. Commun.*, 4, 2188, 2013.

[3] J. Labuta, S. Ishihara, A. Shundo, S. Arai, S. Takeoka, K. Ariga and J. P. Hill, "Chirality Sensing by Nonchiral Porphines", *Chem. Eur. J.*, *17*, 3558, 2011.

[4] V. Březina, S. Ishihara, J. Lang, L. Hanyková, K. Ariga, J. P. Hill, J. Labuta. "Structural Modulation of Chromic Response: Effects of Binding-Site Blocking in a Conjugated Calix[4]pyrrole Chromophore", *ChemistryOpen*, *7*, 323,2018.

[5] A. Shundo, S. Ishihara, J. Labuta, Y. Onuma, H. Sakai, M. Abe, K. Ariga and J. P. Hill, " Colorimetric Visualization of Acid–base Equilibria in Non-polar Solvent" *Chem. Commun.*, *49*, 6870, 2013.

[6] S. Ishihara, J. Labuta, T. Šikorský, J. V. Burda, N. Okamoto, H. Abe, et al., "Colorimetric Detection of Trace Water in Tetrahydrofuran Using N,N'-Substituted Oxoporphyrinogens", *Chem. Commun.*, *48*, 3933, 2012.

[7] J. Labuta, Z. Futera, S. Ishihara, H. Kouřilová, Y. Tateyama, K. Ariga and J. P. Hill, "Chiral Guest Binding as a Probe of Macrocycle Dynamics and Tautomerism in a Conjugated Tetrapyrrole", *J. Am. Chem. Soc.*, *136*, 2112, 2014.

RESEARCH AND FABRICATION OF SURFACE-ENHANCED RAMAN SCATTERING – SERS BASED ON STRUCTURE OF ZnO NANOROD/Ag THIN FILMS

Tran Đo Minh Hoang, Nguyen Hoang Long, Truong Duc Nguyen, Nguyen Ha Thanh, Đao Anh Tuan, Le Vu Tuan Hung

Faculty of Physics, University of Sciences, Vietnam National University Ho Chi Minh City

*Email:

In recent years, the new method that can detect chemical compounds at very low concentrations is the enhancement Raman signals by surface plasmon resonance effect – SERS method. SERS is attracted by many scientists because it helps to identify molecules easily and quickly at very low concentrations, but still does not destroy samples or discolor the samples. So it is used in many fields such as physics, nanotechnology, chemistry, biology ... In this study, we fabricated SERS substrate based on nano Ag-decorated ZnO nanorod array. Firstly, we synthesized ZnO nanorods by sol-gel method and wet chemical method, then proceeded to modify Ag thin films on ZnO nanorods by DC magnetron sputtering method. We also investigated the change in film thickness and the heating time of nano Ag to obtain the optimal Raman signal as they were used to detect Rhodamine 6G (R6G) at concentrations >10^{-6} M

Keywords: SERS, The enhancement factor, ZnO nanorods, nano films Ag, Rhodamine 6G, ...

ELECTRON PARAMAGNETIC STUDY OF MN^{2+}/CR^{3+} DOPED ZNO NANOPARTICLES WITH ENHANCED PHOTOCATALYTIC ACTIVITY

Nguyen Xuan Sang[1,*], Vo Cao Minh[1], Phan Tan Dat[1], Do Huu Quyet[2], Trinh Xuan Thang[2]

[1]Saigon University, 273 An Duong Vuong, ward 3, district 5, Ho Chi Minh City 700000, Vietnam
[2]Research Laboratories of Saigon High-Tech-Park, Lot I3, N2 Street, Saigon Hi-Tech-Park, district 9, Ho Chi Minh city 700000, Vietnam
*Email: sangnguyen@sgu.edu.vn

ZnO nanoparticle doped transition ion Mn^{2+}/Cr^{3+} was synthesized by a solgel method. The nature of the point defect of dopants was analyzed by electron spin resonance (ESR) and photoluminescence (PL) emission which revealed the role and the site distribution of ions in the enhancement of the photocatalytic activity. In general, when the dopant content was increased, the PL intensity was sharply reduced. The result indicated the longer life time of excited carriers which was due to the formation of a heterojunction between the dopant ions and ZnO. In ZnO:Cr^{3+} samples, the typical ESR signal with a g-factor ~1.96 was completely passivated, indicating the diffusion of electrons near the conduction band into the dopant ions. The doped Cr^{3+} ion acts as an electron trap in the ZnO crystal. In ZnO:Mn^{2+}, characteristic ESR signals from ion Mn in crystal were indicated site distribution of the dopant such as substitutional, interstitial, and cluster sites. Furthermore, the mechanism for enhancing the photocatalytic activity of doped ZnO was proposed in respect of point defect evolution through the doping manner.

Key words: ZnO, point defect, electron spin resonance, transition metal ions

INTRODUCTION

Background

Doped semiconductor technology has been received a huge attention from scientists worldwide due to novel and excited properties could be achieved from traditional semiconductors such as optics, magnetics, biosensors [1-5]. Zinc oxide (ZnO) is one the most studied oxide semiconductor because of its natural abundance, environmental friendly, and it owns genius electronic characteristics, i.e. wide direct bandgap (3.3 eV), large exciton binding at room temperature (30 meV). Recently, researchers pay a lot of attention on ZnO for photocatalytic activity by doping ZnO with another transition metal ions to reduce recombination rate of electron-hole pair by forming heterojunction between the host matrix and the dopant [1, 6-9]. Many fabrication techniques were successful to dope ZnO with transition metal ions, one of the simplest method with strong advances is sol-gel method. This technique is quite simple and the production was normally in a uniform shape. Although many works have been done, the behavior and atomic-scale of dopant investigation was not enough to bring a clear view of dopant site in the host. In this work, we investigate the effect of Mn and Cr dopant on electronic properties of ZnO and give more details in site distribution of Mn ion which revealed by electron spin resonance study. Furthermore, a sunlight irradiation induced photocatalytic activity of synthesized samples was evaluated by the degradation of methylene blue.

RESULTS

Fig. 1 shows TEM images of synthesized samples ZnO, ZnO:Cr5%, and ZnO:Mn5%. The synthesized samples were in particle shape with homogenous in size. The particle size was gradually decreased in doped samples, ~15 nm for ZnO, ~8 nm for ZnO:Cr5%, and ~10 nm for ZnO:Mn5%.

Figure 1: (From left-hand side) Transmission electron microscopy images of ZnO, ZnO:Cr5%, and ZnO:Mn5%; scale-bar 20nm

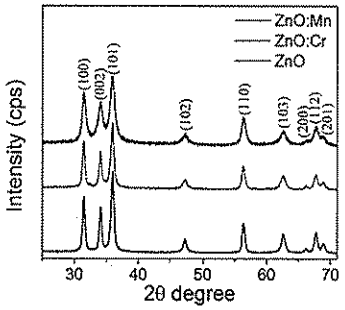

Figure 2: X-ray diffraction patterns of ZnO, ZnO:Cr, and ZnO:Mn samples.

X-ray diffraction patterns of these samples are shown in fig. 2 which indicate that all sample are in wurtzite structure with 2θ at 31.5°, 34.12°, 35.97°, 47.28°, 56.38°, 62.62°, 66.19°, 67.74°, and 68.90°, corresponding to the faces (100), (002), (101), (102), (110), (103), (200), (112), (201) (JCPDS File No.36-1451) and no secondary phase revealed, the patterns have an agreement with TEM images in terms of particle size.

Electron spin resonance (ESR) is a powerful technique to identify paramagnetic point defect in semiconductor based on dangling bonds of unpaired electrons. Characteristic ESR signals of ZnO at g value of 1.96 and 2.003 were reported previously and their origins have not yet fully understood. Vanheusden [13] assigned signal at g = 1.96 from oxygen vacancy. This proposal was widely accepted in various studies however, recently, in a series of ZnO nanoparticle study of Erdem and co-workers [14, 15] was proposed a core-shell model which assigned 1.96 signal as zinc interstitial from core-defect, and 2.003 signal as oxygen vacancy from shell-defect. In our study, these signals were appeared in the pure ZnO as shown in fig. 3. However, the g = 1.96 was completely passivated and the g = 2.003 still remained. The passivation process in the presence of ion Cr^{3+} may due to the reduction activity of ion Cr capture ZnO excessive electron to form lower oxidation states. Hence, the g =1.96 origin is likely from electron near the conduction band, which is in agreement to the work of Jannoti [16].

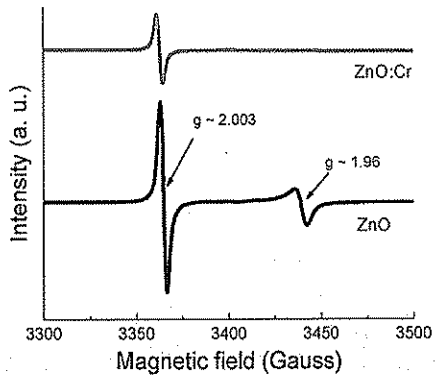

Figure 3: Room temperature X-band electron spin resonance spectra of ZnO and ZnO:Cr^{3+}.

For ion Mn doped ZnO, Mn^{2+} has 5/2 nuclear spin number (I = 5/2, ~100% abundance) and 5 electrons in outer shell (S=5/2), the ESR signal of Mn^{2+} is more complicated with allowed transition ($\Delta m_S = \pm 1$) give rise to 6 convolution peaks as hyperfine interaction. Moreover, the interaction among electrons also contributes to ESR signal as finestructure. Figure 4 shows ESR signal of Mn doped ZnO samples with various contents of Mn ion. Fortunately, Mn sites such as substitutional, interstitial, and cluster could be identified by ESR study [17]. We can profile site distribution of Mn ion in ZnO. It indicated that the doping difficulty that doping efficiency could not increase by increasing the content of Mn ion.

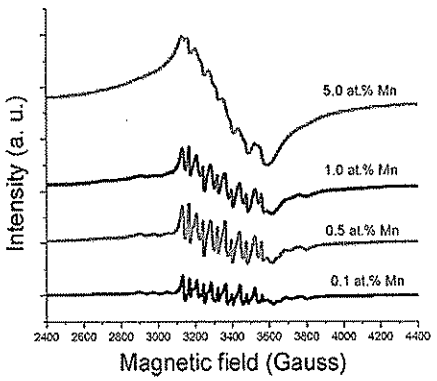

Figure 4: Room temperature X-band electron spin resonance spectra of ZnO and ZnO:Mn^{2+} samples.

In this part, we evaluated photocatalytic activity of synthesized samples by measuring the degradation of methylene blue solution under direct sunlight. Figure 5 showed the photocatalytic ability of ZnO, ZnO:Cr, and ZnO:Mn. When doped, materials have a better photocatalytic performance due to heterojunction between the dopant and the crystal host. Mechanism of the enhancement could be found in various studies [1, 18].

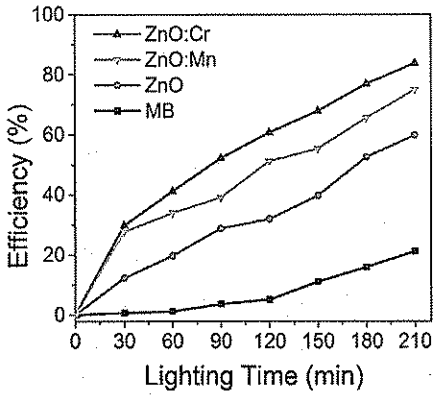

Figure 5: Photocatalytic activity in degradation methylene blue under direct sunlight of ZnO, ZnO:Cr, and ZnO:Mn.

CONCLUSION

We have identified the electronic structure evolution of zno doped transition metal ion (cr^{3+}, mn^{2+}). Electron-rich in nanoparticle zno contributed to the g = 1.96 signal which was completely passivated by ion cr^{3+}. By simulation the esr signal of mn^{2+}, we could calculate site distribution of mn^{2+} in the host crystal. Photocatalytic activity was carried out and showed the improvement of zno doped materials.

ACKNOWLEDGEMENTS

This research is partially funded by Saigon University Foundation for Research under Grant Number CS2019-46.

REFERENCES

[1] F. Achouri, S. Corbel, L. Balan, K. Mozet, E. Girot, G. Medjahdi, M.B. Said, A. Ghrabi, R. Schneider, Porous Mn-doped ZnO nanoparticles for enhanced solar and visible light photocatalysis, Materials & Design, 101 (2016) 309-316.

[2] O. Altintas Yildirim, H. Arslan, S. Sönmezoğlu, Facile synthesis of cobalt-doped zinc oxide thin films for highly efficient visible light photocatalysts, Applied Surface Science, 390 (2016) 111-121.

[3] D. Chu, Y.-P. Zeng, D. Jiang, Synthesis and growth mechanism of Cr-doped ZnO single-crystalline nanowires, Solid State Communications, 143 (2007) 308-312.

[4] R. Janisch, P. Gopal, N.A. Spaldin, Transition metal-doped TiO2and ZnO—present status of the field, Journal of Physics: Condensed Matter, 17 (2005) R657-R689.

[5] H. Mirzaei, M. Darroudi, Zinc oxide nanoparticles: Biological synthesis and biomedical applications, Ceramics International, 43 (2017) 907-914.

[6] S. Choi, J.Y. Do, J.H. Lee, C.S. Ra, S.K. Kim, M. Kang, Optical properties of Cu-incorporated ZnO (Cu x Zn y O) nanoparticles and their photocatalytic hydrogen production performances, Materials Chemistry and Physics, 205 (2018) 206-209.

[7] M.F. Khan, A.H. Ansari, M. Hameedullah, E. Ahmad, F.M. Husain, Q. Zia, U. Baig, M.R. Zaheer, M.M. Alam, A.M. Khan, Z.A. AlOthman, I. Ahmad, G.M. Ashraf, G. Aliev, Sol-gel synthesis of thorn-like ZnO nanoparticles endorsing mechanical stirring effect and their antimicrobial activities: Potential role as nano-antibiotics, Scientific reports, 6 (2016) 27689.

[8] Y. Liu, J. Yang, Q. Guan, L. Yang, Y. Zhang, Y. Wang, B. Feng, J. Cao, X. Liu, Y. Yang, M. Wei, Effects of Cr-doping on the optical and magnetic properties in ZnO nanoparticles prepared by sol–gel method, Journal of Alloys and Compounds, 486 (2009) 835-838.

[9] T.N. Ravishankar, K. Manjunatha, T. Ramakrishnappa, G. Nagaraju, D. Kumar, S. Sarakar, B.S. Anandakumar, G.T. Chandrappa, V. Reddy, J. Dupont, Comparison of the photocatalytic degradation of trypan blue by undoped and silver-doped zinc oxide nanoparticles, Materials Science in Semiconductor Processing, 26 (2014) 7-17.

[10] M.F. Acosta Humánez, L.A. Montes Vides, O.A. Almanza-Montero, Sol-gel synthesis of zinc oxide nanoparticle at three different temperatures and its characterization via XRD, IR and EPR, Dyna, 83 (2016) 224-228.

[11] J.N. Hasnidawani, H.N. Azlina, H. Norita, N.N. Bonnia, S. Ratim, E.S. Ali, Synthesis of ZnO Nanostructures Using Sol-Gel Method, Procedia Chemistry, 19 (2016) 211-216.

[12] N.X. Sang, P.T.L. Huong, T.T.M. Thy, P.T. Dat, V.C. Minh, N.H. Tho, Crystalline deformation and photoluminescence of titanium dioxide nanotubes during in situ hybridization with graphene: An example of the heterogeneous photocatalyst, Superlattices and Microstructures, (2018).

[13] K. Vanheusden, C.H. Seager, W.L. Warren, D.R. Tallant, J.A. Voigt, Correlation between photoluminescence and oxygen vacancies in ZnO phosphors, Applied Physics Letters, 68 (1996) 403-405.

[14] E. Erdem, Microwave power, temperature, atmospheric and light dependence of intrinsic defects in ZnO nanoparticles: A study of electron paramagnetic resonance (EPR) spectroscopy, Journal of Alloys and Compounds, 605 (2014) 34-44.

[15] S. Repp, E. Erdem, Controlling the exciton energy of zinc oxide (ZnO) quantum dots by changing the confinement conditions, Spectrochimica acta. Part A, Molecular and biomolecular spectroscopy, 152 (2016) 637-644.

[16] A. Janotti, C.G. Van de Walle, Fundamentals of zinc oxide as a semiconductor, Reports on Progress in Physics, 72 (2009) 126501.

[17] L. Chen, D. Kirilenko, A. Stesmans, X.S. Nguyen, K. Binnemans, B. Goderis, J. Vanacken, O. Lebedev, G. Van Tendeloo, V.V. Moshchalkov, Symmetry and electronic states of Mn2+ in ZnS nanowires with mixed hexagonal and cubic stacking, Applied Physics Letters, 97

(2010) 041918.
[18] M.R.D. Khaki, M.S. Shafeeyan, A.A.A. Raman, W. Daud, Application of doped photocatalysts for organic pollutant degradation - A review, Journal of environmental management, 198 (2017) 78-94.
, B. Author, "Proceedings Title", in *Conference Name*, Tokyo, June 8-12, 2015, pp. 10-15.
[2] A. Author, B. Author, "Paper Title", *Journal Name*, vol. 7, pp. 100-110, 2000.
[3] C. Author, *Book name*, Publisher Name, 2000.

POROUS FULLERNE NANOMATERIALS FOR VOC SENSING

Lok Kumar Shrestha[1,*] Katsuhiko Ariga[1,2]
[1]International Center for Materials Nanoarchitectonics (WPI-MANA), National Institute for Materials Science (NIMS), 1-1 Namiki, Ibaraki Tsukuba 305-0044, Japan; [2] Graduate School of Frontier Science, The University of Tokyo, Kashiwa, Chiba 277-0827, Japan

*Email: SHRESTHA.Lokkumar@nims.go.jp

We report the production of self-assembled fullerene nanomaterials from zero to higher dimensions including porous fullerene crystals using liquid-liquid interfacial precipitation method. Due to the enhanced surface area and porosity, our material showed excellent VOC sensing performance sensitive towards aromatic solvents. This is due to easy and free diffusion of aromatic solvent vapors into the nanopores utilizing π-π interaction between solvent molecules and sp^2-bonded π-electron rich carbon frameworks.

Key words: fullerene, self-assembly, micropores, mesopores, VOC sensing

INTRODUCTION

Background

Fullerene is a π-electron rich nanocarbon material with interesting properties such as high hydrophobicity, strong van der Waals and π–π interactions derived from its fused π-conjugated structure [1]. Contrary to the many organic materials, fullerene potentially form various self-organized structures [2-5]. Design of hierarchy and porous structure will enhance the surface area and active adsorption site for the targeted gas molecules [6]. Furthermore, composite with metal or metal oxides will promote adsorption of noxious vapors via charge-transfer interactions. It is expected that the self-organized hierarchical fullerene nanomaterials with porous (micro- and mesopores) structure and composite with metal oxides would be the excellent sensing materials (host) for aromatic vapors.

In this contribution, we will discuss the simple solution-based strategy for the fabrication of fullerene nanostructures from zero to higher dimensions including mesoporous fullerene nanosheets and microcubes. Furthermore, we will discuss the recently developed technique to dimension-dependent face-selective chemical etching of self-assembled fullerene nanostructures in solution, which mimic the molecular beaker lithography.

RESULTS

Using a liquid-liquid interfacial precipitation method under different combinations of good and poor solvent of fullerenes, we have successfully produced dimensionally-integrated self-assembled fullerene nano/micro crystals (Figure 1).

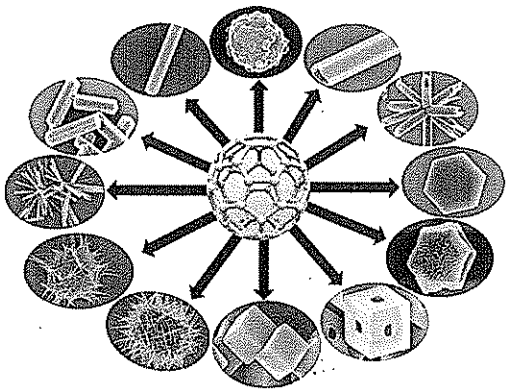

Figure 1. *Self-assembled fullerene crystals from zero to higher dimensions prepared by solution based strategy (liquid-liquid interfacial precipitation method).*

Most of these self-assembled fullerene crystals are solid solvates containing solvated solvent molecules. Intentional heat-treatment just above the boiling temperature of solvated solvent resulted in the formation of porous structure. As a separate strategy to design porous fullerene nanomaterials, we grew crystals from the mixed solvents system. For example, when crystal is grown from a fullerene solution in the mixture of toluene and carbon tetrachloride using isopropanol as poor solvent, fullerene nanosheets with bimodal pore architecture are formed [7]. The pore formation mechanism is based on the fact that toluene entrapped in the crystal during fast crystallization tends to release out of the crystal as it does not stabilize solid solvates.

We have also succeeded to demonstrate the face-selective chemical etching of the fullerene crystals with ethylene diamine (EDA) under the ambient condition of temperature that leads to the formation of porous EDA functionalized fullerene nanomaterials. EDA selectively etched through both ends of the fullerene nanorods resulting in the formation of hollow tubular structure. While, etching was rather isotropic in case of fullerene cubes and resulted in the formation of gyroid-shape porous object. These chemically

etched porous fullerene nanostructure showed excellent vapor sensing performance selective to acid vapors (formic and acetic acid) compared to aromatic vapors (benzene or toluene). This is a simple and scalable solution process to construct hollow and hierarchical fullerene nanostructures, which would be very useful in biological, ionic sensing, separation, and energy storage and drug carrier applications.

CONCLUSION

In conclusions, we have prepared fullerene-based nanomaterials from zero to higher dimensions using a simple solution based strategy called liquid-liquid interfacial precipitation method. We have established a new and template-free method for the production of porous fullerene nanomaterials, which show superior VOC sensing performance selective to either aromatic vapors compared to the commercial active carbons. Furthermore, we have also successfully demonstrated face-selective chemical etching of the self-assembled fullerene nanomaterials. Despite the costly lithography technique, this is a simple and scalable solution process, which is very cheap strategy that mimic molecular beaker lithography to construct hollow fullerene nanostructures. The chemically etched fullerene-based nanomaterials show excellent sensing performance selective towards acid vapors due to surface functionalization of basic amines.

ACKNOWLEDGEMENTS

This study was partially supported by JSPS KAKENHI Grant Number JP16H06518 (Coordination Asymmetry) and CREST JST Grant Number JPMJCR1665.

REFERENCES

[1] H. W. Kroto, J. R. Heath, S. C. O'Brien, R. F. Curl, R. E. Smalley, C60: Buckminsterfullerene. Nature **1985**, *318*, 162-163.

[2] L. K. Shrestha, Q. Ji, T. Mori, K. Miyazawa, Y. Yamauchi, J. P. Hill, K. Ariga, Fullerene Nanoarchitectonics: From Zero to Higher Dimensions. *Chem. –Asian J.* **2013**, *8*, 1662-1679.

[3] P. Bairi, K. Minami, J. P. Hill, W. Nakanishi, L. K. Shrestha, C. Liu, K. Harano, E. Nakamura, K. Ariga, Supramolecular Differentiation for Construction of Anisotropic Fullerene Nanostructures by Time-Programmed Control of Interfacial Growth. *ACS Nano*, **2016**, *10*, 8796-8802.

[4] P. Bairi, T. Tsuruoka, S. Acharya, Q. Ji, J. P. Hill, K. Ariga, Y. Yamauchi and L. K. Shrestha, Mesoporous Fullerene C70 Cubes with Highly Crystalline Frameworks and Unusually Enhanced Photoluminescence Properties. *Mater. Horiz.* **2018**, *5*, 285-290.

[5] P. Bairi, K. Minami, J. P. Hill, K. Ariga and L. K. Shrestha, Intentional Closing/Opening of "Hole-in-Cube" Fullerene Crystals with Microscopic Recognition Properties. *ACS Nano*, **2017**, *11*, 7790-7796.

[6] P. Bairi, K. Minami, W. Nakanishi, J. P. Hill, K. Ariga, L. K. Shrestha, Hierarchically Structured Fullerene C70 Cube for Sensing Volatile Aromatic Solvent Vapors, *ACS Nano.* **2016**, *10*, 6631-6637.

[7] L. K. Shrestha, Y. Yamauchi, J. P. Hill, K. Miyazawa and K. Ariga, Fullerene Crystals with Bimodal Pore Architectures Consisting of Macropores and Mesopores. *J. Am. Chem. Soc.*, **2013**, *135*, 586-589.

PLASMON-MEDIATED CHEMICAL REACTION AT THE NANOSCALE FOR SENSING DEVICE AND CATALYST PREPARATION

Mai T.T. Nguyen[1,*], Nordin Felidj[2], Claire Mangeney[3], Ly T. Le[4], Phong D. Tran[4]
[1]Hanoi University of Science and Technology (Vietnam); [2]University Paris Diderot (France); [3]University Paris 05 (France); [4]University of Science and Technology of Hanoi, Vietnam Academy of Science and Technology (Vietnam)
*Email: mai.nguyenthituyet1@hust.edu.vn

ABSTRACT

Plasmonic nanoparticles (NPs) have been the subject of extensive research, due to their remarkable optical properties. In chemistry, plasmonic NPs can offer a unique platform to selectively boost the chemical reaction yields with a spatial control at the nanoscale. In our works, a plasmon-mediated grafting of aryl films derived from diazonium salts on Au-NPs array was demonstrated. This grafting occurs specifically in the regions of maximum of field enhancement. It could provide a general strategy to attach molecules to hot spot regions and further improve their detection for sensing applications.

On the other hand, a Au-NPs@MoS_x core@shell structure was prepared by using an innovative plasmon-driven redox reaction. We show that the Au-NPs@MoSx displays an attractive catalytic activity for the hydrogen evolution reaction in water. Interestingly, removing the MoS_x shell exposes the Au-NPs core that displays even superior catalytic activity. Therefore, Au-NPs could be considered as an attractive alternative to Pt catalysts for engineering a photoelectrode for a PEC device for solar H_2 generation.

Key words: Plasmonics, gold nanoparticles, catalyst, hydrogen generation

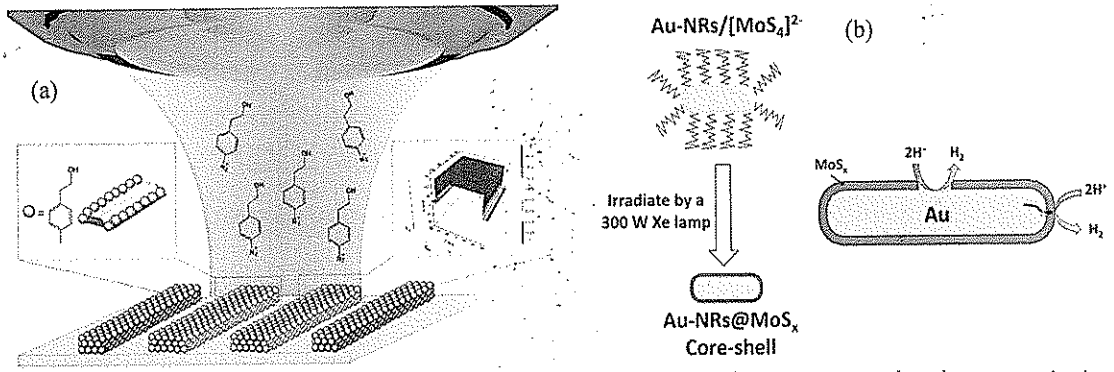

Figure 1: Schemes of the regioselective surface functionalization of gold nanostripes under plasmon excitation (a) and the preparing Au-NRs@MoS_x core@shell catalyst by plasmon-driven approach.

REFERENCES

[1] Tien D. Tran et al., *Chem. Commun.* **2018**, 54, 3363-3366
[2] Tijunelyte I. et al, *Nanoscale Horizons* **2018**, 3, 53-57
[3] Nguyen M. et al., *Nanoscale* **2016**, *8*, 8633-8640.
[4] Nguyen M. et al. *Chem. Commun.* **2017**, *53*, 11364-11367.

GAS SENSING PROPERTIES OF MG-INCORPORATED METAL-ORGANIC FRAMEWORKS

Jae-Hyoung Lee[1,†], Thanh-Binh Nguyen[2,†], Duy-Khoi Nguyen[3], Jae-Hun Kim[1], Jin-Young Kim[1], Bach Thang Phan[3,*], and Sang Sub Kim[1,*]

[1]Department of Materials Science and Engineering, Inha University, Incheon 22212, Republic of Korea
[2]Faculty of Chemistry, Ho Chi Minh City University of Education, Ho Chi Minh City 721337, Vietnam

[3]Center for Innovative Materials and Architectures (INOMAR), Vietnam National University, Ho Chi Minh City 721337, Vietnam

The gas sensing properties of two novel series of Mg-incorporated metal–organic frameworks (MOFs), termed Mg-MOFs-I and -II, were assessed. The synthesized iso-reticular type Mg-MOFs exhibited good crystallinity, high thermal stability, needle-shape morphology and high surface area (up to 2900 $m^2 \cdot g^{-1}$), which are promising for gas sensing applications. Gas-sensing studies of gas sensors fabricated from Mg-MOFs-II revealed better sensing performance, in terms of the sensor dynamics and sensor response, at an optimal operating temperature of 200 °C. The MOF gas sensor with a larger pore size and volume showed shorter response and recovery times, demonstrating the importance of the pore size and volume on the kinetic properties of MOF-based gas sensors. The gas-sensing results obtained in this study highlight the potential of Mg-MOFs gas sensors for the practical monitoring of toxic gases in a range of environments.

Key words: Mg-MOF; gas sensor; porosity; toxic gas; sensing mechanism

* Correspondence: pbthang@inomar.edu.vn (B.T.P.); sangsub@inha.ac.kr (S.S.K.); Tel.: +84-79-790-7700 (B.T.P.); Tel.: +82-32-860-7546 (S.S.K.)

†Jae-Hyoung Lee and Thanh-Binh Nguyen contributed equally to this work.

IN-SITU HYBRIDIZATION GRAPHENE NANOFLAKE WITH TUNGSTEN OXIDE NANOBRICK FOR LOW POWER CONSUMPTION NH_3 GAS SENSOR

Nguyen Huu Lam[1], Luu Thi Lan Anh[1], Nguyen Cong Tu[1,*]
[1]School of Engineerig Physics, Hanoi University of Science and Technology, No 1 Dai Co Viet, Hanoi
*Email: tu.nguyencong@hust.edu.vn

ABSTRACT

In-situ Gr@WO_3 nanobricks hybrid nanomaterials are synthesized by direct dispersing graphene nanoflakes (0.1, 0.3 and 0.5 wt.%) into precursor solution of tungsten oxide prepared by hydrothermal method at 180 °C for 48h. The resistance of resisitive hybrid material-based sensor decrease with the content of graphene flake. The ammonia gas sensing characteristics of hybrid material-based sensors is investigated at 250 °C. The 0.5 wt.% Gr@WO_3 - based gas sensor shows highest response, shorter recovery time, but longer response time. The morphology and crystal structure of nanostructures are examined through analyzing FESEM images, XRD patterns, and Raman scattering spectra. The strong interaction between graphene and tungsten oxide is characterized by XRD and Raman analysis.

Keywords: graphene nanoflake, tungsten oxide nanobrick, gas sensor, hybrid material.

QUARTZ CRYSTAL MICROBALANCE (QCM) BIOSENSOR BASED ON GOLD NANOBIPYRAMIDS AMPLIFICATION FOR CHLORAMPHENICOL RESIDUAL DETECTION.

Trong Phat Huynh[1,*], Vo Ke Thanh Ngo[1], Dang Giang Nguyen[1]
[1] Research Laboratories of Saigon Hi-tech Park
*Email: phat.huynhtrong@shtplabs.org

In recent years, biosensors which based on quartz crystal microbalance (QCM) for chemical and biological detections were researched. The advantages of QCM biosensors are rapid, cheap and easy to use. However, they still have some disadvantages such as not stable and low sensitive. So that, it is hardly to detect the small molecular weight target. In this work, we develop a QCM biosensor to detect chloramphenicol residues. Gold nanobipyramids (NBPs) were used to amplifying the sensitive of QCM biosensors. The low chloramphenicol concentration from 0.1-1.5 ppm can be detected this biosensor. Quartz crystal microbalance biosensor has promising for further applications such as food safety and environment detection.

Key words: quartz crystal microbalance, biosensor, gold nanobypiramids.

INTRODUCTION

Background

Antibiotic residues are molecules that remain in meat from animals been treated with antibiotics. They may be pose adverse health effects for the consumer [1].

Chloramphenicol (CAP) is an efficient antibiotic with broad spectrum activity which is used in both human, veterinary medicine. Also its use was extended for the treatment of typhoid fever, meningitis, cholera and rickets diseases. However, CAP has displayed serious toxic side effects on humans and animals, such as granulocytopenia, aplastic anaemia, thrombocytopenia and the "gray baby syndrome" [2]. Hence, most countries, including China, the United States, and European Union countries, have strictly prohibited its applications in agriculture and aquaculture products [3]. Thus, the detection in food products is highly important. Currently used methods for the detection of CAP include immunorassay, microbiological method, GC-MS an LC-MS. These methods are expensive, complicated and long time responding. Hence, cheap, rapid and easy methods for CAP detection are important.

Quartz crystal microbalances 5 Mhz (Figure 1) were fabricated at SHTP's labs. The crystal resonance frequency will decrease with an increase in mass on the surface of electrode. The relationship between the frequency changing and mass loading is described by equation below [4]:

$$\Delta f = -22.6 \times 10^{-6} \Delta m \frac{f^2}{A}$$

There Δf is frequency changing, Δm is mass loading on electrode surface, A is area of QCM. If Δm is very small, Δf will be slight change. In order to improve the sensitive of QCM biosensor, conjugated Au nanoparticles can be used to amplify the frequency change. Normally, spherical gold nanoparticles are used as "mass enhancers" but the sensitive is not significant because of their small weigh. In this report, we use gold nanobipyramids, an advance nanomaterials, to amplify the signal of QCM biosensor to detect CAP at low concentration.

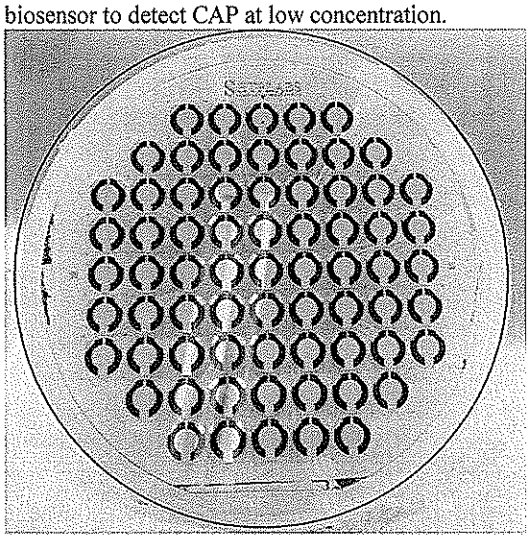

Figure 1: QCM fabricated in SHTP's Labs

Experiments

Gold nanobipyramids were preparated by seed-mediated method using microwave irradiation enhanced. The surface of NBPs were modified by thiol polyethylene glycol (PEG-SH) as stabilizers. The CAP antibodies were conjugated onto QCM surface by SAM method using glutaraldehyde, thiourea. QCM biosensor measurements were performed by Seiko – QCM 934 system (Figure 2).

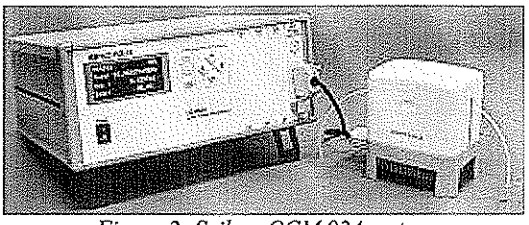

Figure 2: Seiko - QCM 934 system

RESULTS

Characterization of NBPs

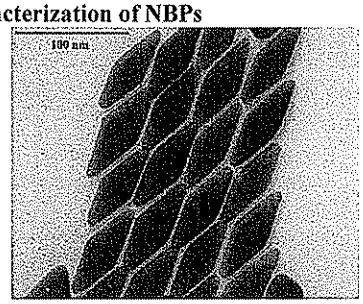

Figure 3: TEM of NBPs

Gold nanobipyramids (88.4 nm ± 9.4 nm in length and 29.9 nm ± 3.2 in diameter) were prepared using microwave irradiated at 800W microwave powers for 15 minutes (Figure 3).

The comparison of frequencies changing of with and without NBPs amplified QCM biosensors was shown in figure 4. Both frequencies were changed when the concentrations of CAP were 0.5 ppm. But the frequency's attenuation of NBPs amplification (526 Hz) is more 7 times than QCM biosensor (75 Hz). However, the CAP concentration was ≤0.1ppm, the temporal response curves of QCM biosensor could not distinguish from the baseline of negative control (about 10 Hz). Because of low concentration, CAP molecule numbers captured by specific antibodies are not enough to make a remarkable frequency change.

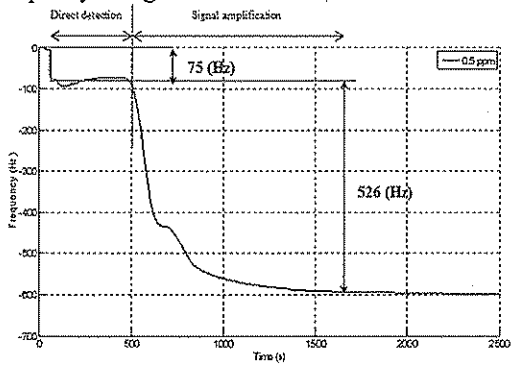

Figure 4: The frequency's attenuation of without and with amplification QCM biosensor at CAP 0.5 ppm

Figure 5 is shown the response of QCM biosensor using NBPS amplification. We found that frequencies decrease quickly when CAP concentrations increase from 0.1 ppm to 1.5 ppm. The higher concentration is, the greater the sensor response is.

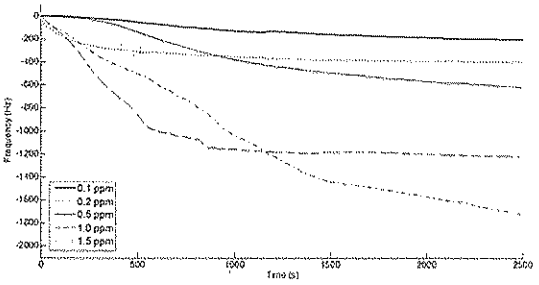

Figure 5: The frequency's attenuations of NBPs amplification in different CAP concentrations

The more CAP molecules have been captured by specific antibodies, the more the mass covered the surface of the Au electrode, and then the more frequency shift of measurement decreased. The change of frequencies is a linear line in range 0.1-1.5 ppm, this result allows QCM system to be used for qualitative and quantitative analysis of CAP residual (Figure 6). QCM immunsensor have fast response time, about 1 h. Current rapid screening methods such as PCR and HPLC still need sample enrichment to get a detectable CAP concentration, taking 8–20 h. The described QCM immunsensor with nanoparticle amplification could be a promising alternative to these methods.

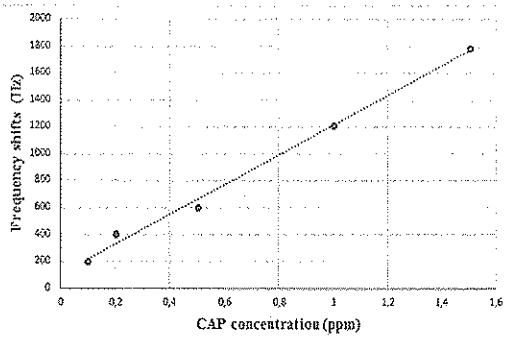

Figure 6: Frequencies changing of biosensor by CAP concentrations

CONCLUSION

In our study, gold nanobipyramids were successfully prepared by microwave irradiation. NBPs have been applied in signal amplification for QCM biosensor. As low as CAP concentration could be detected by this method. This is a promising method to use in food safety and environment monitoring.

REFERENCES

[1] T. Ramatla, L. Ngoma, M. Adetunji, M.

Mwanza1, "Evaluation of Antibiotic Residues in Raw Meat Using Different Analytical Methods", *Antibiotics (Basel)*, vol. 6, pp. 34-51, 2017 .

[2] E.M.M.Niang, A.M.Assoum, A.Teko Agbo, K.Akoda, A.Talnan, S.O.Sarr, "Chloramphenicol residue levels of marketed farm gate milk in Senegal", *Food Control*, vol. 72, pp. 249-254, 2017.

[3] X. Shi , S. Song, A. Sun, D. Li, A. Wu, D. Zhang, "Determination of Chloramphenicol Residues in Foods by ELISA and LC-MS/MS Coupled with Molecularly Imprinted Solid Phase Extraction", *Journal Analytical Letters*, vol. 43, pp. 2798-2807, 2010.

[4] L. Wang, Q. Wei , C. Wut, J. Ji, P. Wang, "Proceedings of International Conference on Information Acquisition", Jeju City, July 9-11, 2007, pp. 46-51.

NANO SELF-ASSEMPBLE POLY(ARGININE)-BASED REDOX INJECTABLE HYDROGEL FOR THERAPEUTIC APPLICATION IN MYOCARDIAL INFARCTION

Long Binh Vong[1,2*], Yukio Nagasaki[2,3,4]
[1]Department of Biomedical Engineering, International University, Vietnam National University Ho Chi Minh city; [2]Department of Materials Science, University of Tsukuba
[3]Department of Medical Sciences, University of Tsukuba; [4]CRiED, University of Tsukuba
*Email: vblong@hcmiu.edu.vn

Nitric oxide (NO) possesses various functions in cardiovascular diseases. Here, we newly designed a nano/poly(arginine)-based injectable hydrogel (NO-RIG) to maintain the NO release in myocardiac tissue. NO-RIG possesses ROS scavenging capacity to improve NO bioavailability. The NO-induced angiogenesis was remarkably observed in mice treated with NO-RIG. Using a murine myocardial infarction (MI) model and other control injectable gels, we found only the mice treated with NO-RIG showed statistically significant recovery of cardiac functions in both severe and moderate MI models. Our results clearly indicate that treatment with NO-RIG effectively control the NO generation and angiogenesis induction *in vivo*.

Key words: redox injectable hydrogel, nano self-assembly drug, nitric oxide, cardiovascular disease

INTRODUCTION

Myocardial infarction (MI) is characterized by necrosis of myocardial tissue due to ischemia, and overproduction of reactive oxygen species (ROS) in ischemic myocardium. Nitric oxide (NO), small gas molecule, has been reported to play a critical role in cardiovascular disease. Although NO therapy improves blood flow and neovascularization after MI, due to very short half-life and non-specific diffusion, it would be a big limitation for delivery of NO and low-molecular-weight NO donors as therapy. In addition, ROS in ischemic myocardium facilely interact with NO to form peroxynitrite ($ONOO^-$), which further causes tissue damage and suppresses the NO availability. Recently, we have developed a controllable NO releasing self-assemble nanoparticle using macrophage-targeted poly(arginine) (PArg) for immuno-cancer therapy[1]. We previously also developed ROS scavenging redox polymer, which effectively worked on oxidative stress-related diseases[2,3,4]. In this study, we developed NO/redox injectable hydrogel (NO-RIG) based on formation of polyion complex (PIC) between cationic polymers [ROS scavenging polymer (PMNT-PEG-PMNT) coupled with macrophage-triggered NO releasing polymer (PArg-PEG-PArg)] and anionic polymer [poly(acrylic acid) PAAc] (**Figure 1**) to maintain the NO generation in myocardium after MI for treatment of cardiovascular disease model mice[5].

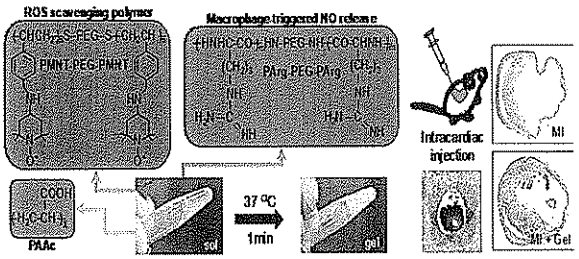

***Figure 1**: Injectable hydrogel (NO-RIG) and its application for myocardial infarction (MI) mice*

RESULTS

The result showed that PIC with the size of around 100 nm displays thermo-irreversible gelation under physiological conditions. Using rheological evaluation, the sol-gel transition was confirmed and occurred at 30-32 °C. The *in vivo* retention of NO-RIG was also evaluated using fluorescent imaging system, and showed that this hydrogel could retain in cardiac tissue at least 10 days after intracardiac injection (**Figure 1**, right). NO-RIG treatment exhibited significantly lowered infarction size in ligation of the left anterior descending artery-induced MI model mice compared to other control injectable hydrogels (**Figure 1**), suggesting that

sustainability of NO release and ROS scavenging properties in cardiac tissue displays an important effect to reduce MI. Using echocardiogram, we could confirm NO-RIG treatment remarkably improved cardiac function of mice such as ejection fraction and fractional shortening parameters. To investigate the therapeutic mechanism by which NO-RIG protects the heart functions after MI, we assessed the induction of angiogenesis by NO-RIG treatment in mouse abdominal skin. The NO-RIG and other control gels were injected intradermally into the abdomen, and the angiogenesis was confirmed at day 7 after injection. To mimic the condition of MI and to activate the immune cells such as macrophages, we used lipopolysaccharide (LPS), which was loaded into the injectable gels. We found that the sham gel and PArg-PIC (NO-IG) treatments did not significantly induce the angiogenesis at all, although a little angiogenesis was observed in mice treated with the LPS-loaded control gel. Interestingly, NO-RIG with LPS treatment clearly induced the angiogenesis in mice, which was significantly higher than in the other treatments (**Figure 2**). Alternatively, it was confirmed that the mice treated with NO-RIG and LPS exhibited a significantly increased production of NO by fluorescent staining of the NO probe with DAF-FM DA. These results clearly indicate that the treatment with NO-RIG can effectively control the NO generation to the desired level in local areas of the diseased tissue, and induces angiogenesis through the activation of macrophages; however, control gel NO-IG did not show any effect.

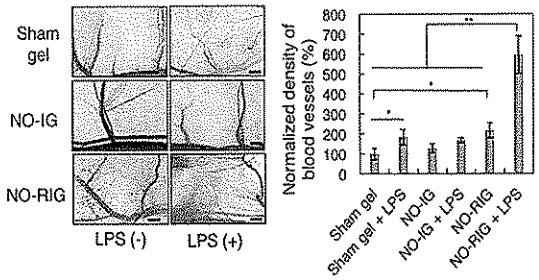

***Figure 2**: NO-RIG treatment induces angiogenesis after intradermal injection as compared to NO-IG (gel has no ROS scavenging capacity). LPS was used to locally activate macrophages.*

CONCLUSION

Taken together, our designed NO-RIG, composed of dual biofunctional triblock polymers, is able to maintain the release of NO and improve its availability coupled with ROS scavenging ability, resulting in inhibition of the progression of MI and improvement of cardiac functions by stimulating the angiogenesis via regulated NO delivery. The results indicate that NO-RIG will be a promising controllable NO releasing hydrogel for treatment of heart failure.

ACKNOWLEDGEMENTS

Authors would like to express sincere appreciation to all collaborators for their supports and valuable advices. This work was partly supported by Young Scientist B (16K16397, JSPS) and NAFOSTED 108.05-2017.327 to L.B. Vong.

REFERENCES

[1] S. Kudo, Y. Nagasaki. A novel nitric oxide-based anticancer therapeutics by macrophage-targeted poly(l-arginine)-based nanoparticles.*Journal of Controlled Release,* 217, 256-262 (2015).

[2] L.B. Vong, T. Yoshitomi, T. Tomita, H. Matsui. Y. Nagasaki. An orally administered redox nanoparticle that accumulates in the colonic mucosa and reduces colitis in mice. *Gastroenterology*, 143, 1027 (2012).

[3] L.B. Vong, T. Yoshitomi, H. Matsui, Y. Nagasaki. Development of an oral nanotherapeutics using redox nanoparticles for treatment of colitis-associated colon cancer. *Biomaterials*, 55, 54-63 (2015).

[4] M.L. Pua, Y. Nagasaki, et al, Redox-active injectable gel using thermo-responsive nanoscale polyion complex flower micelle for noninvasive treatment of local inflammation. *Journal of Controlled Release*, 172, 914-920 (2013).

[5] L. B. Vong, T. Bui, T. Tomita, H. Sakamoto, Y. Hiramatsu, Y. Nagasaki. Novel angiogenesis therapeutics by redox injectable hydrogel - Regulation of local nitric oxide generation for effective cardiovascular therapy. *Biomaterials*,167, 143 (2018

SOLVENT-SPECIFIC PHASE-TRANSITION BEHAVIOR OF A LOW MOLECULAR WEIGHT GELATOR THAT ALLOWS THE DISCRIMINATION OF TOXIC BEVERAGES

Kentaro Tashiro[1,*], Alejandro M. Fracaroli[2]
[1]International Center for Materials Nanoarchitectonics, National Institute for Materials Science; [2]Departamento de Química Orgánica, Universidad Nacional de Córdoba
*Email: TASHIRO.Kentaro@nims.go.jp

Methanol-specific phase-transition behavior of a low molecular weight gelator (LMWG) allows to detect the presence of methanol over the level of regulatory limit in alcoholic drinks (0.1 % according to FDA in USA and MHLW in Japan)[1] through the simple heat-cool treatment of the gel.

Key words: phase-transition, LWMG, methanol

INTRODUCTION

Background

Contamination of beverages, particularly alcoholic drinks with toxic methanol still appears as a fatal issue in the world. While quantification of the methanol content in a beverage sample is typically conducted through the authorized protocols by using GC or HPLC, materials that allow the discrimination of risky beverages in a simple manner could be still attractive under certain circumstances. Here we report an amino-acid based molecule (**1**)[2] whose solvent-specific phase-transition behavior allows to visually detect the presence of methanol over the level of regulatory limit in alcoholic drinks (0.1 % according to FDA in USA and MHLW in Japan).

RESULTS

Molecule **1** was found to form gels in a wide range of organic as well as semi-aqueous solvent conditions. Interestingly, it formed not gels but crystals in methanol or mixtures containing certain amounts of methanol. X-ray crystallography on a single crystal of **1** obtained from pure methanol revealed that stoichiometric amount of methanol with respect to **1** is included as the result of their hydrogen-bonding interaction. The crystal structure also suggests that the observed methanol-specificity of **1** comes fom the size-matching of methanol to fill the spaces in the crystal lattice of **1**, where even ethanol, the second smallest alcohol, is too large for that and eventually directs the gelation of **1**. Addition of a drop of methanol to the gelifiled **1** in acetonitrile or ethyl acetate caused the destruction of the gel to afford a homogeneous solution, demonstrating that the presence of methanol destabilizes the gels.

The methanol-specific phase-transition behavior of **1** inspired us to attempt the visual discrimination of alcoholic drinks contaminated with methanol over the level of regulatory limit by using **1**. When **1** was subjected to the heat-cool treatment in mixtures of water, ethanol, and methanol (alcoholic drink mimics), the gelation behavior of **1** was not sensitive to the amount of methanol, suggesting the competitions among MeOH, EtOH, and water to interact with **1**. On the other hand, by adding the alcoholic drink mimics to **1** in acetonitrile followed by their heat-cool treatment, the sensitivity of the phase-transition behavior of **1** to methanol was much improved, where the methanol concentration down to 0.1% in the alcoholic drink mimic caused the retardation of the gel-formation of **1** (Figure 1).

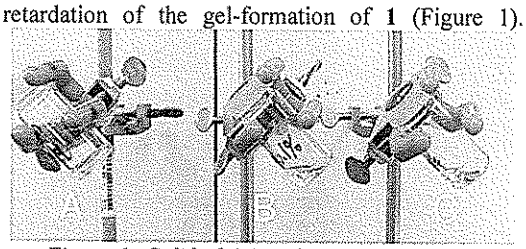

*Figure 1: Gelified (A) and non-gelified (B and C) **1** dependent on the concentration of methanol. Methanol concentrations in the added* alcoholic drink mimics were (A) 0, (B) 0.1, and (C) 1%.

CONCLUSION

By taking advantage of the methanol-specific phase-transition behavior of amino-acid based low molecular weight gelator **1**, we have developed a simple protocol to discriminate alcoholic drinks contaminated with methanol over the level of regulatory limit.

ACKNOWLEDGEMENTS

We thank the invaluable supports of Drs. Richard G. Weiss (Georgetown University) and Felipe Gándara (Materials Science Institute of Madrid) as well as Ms. Girishma Grover (Georgetown University).

REFERENCES

[1] G. Hodson, E. Wilkes, S. Azevedo, T. Battaglene, "Methanol in wine", *BIO Web of Conferences*, vol. 9, pp. 02028, 2017.

[2] A. M. Fracaroli, K. Tashiro, O. M. Yaghi, "Isomers of Metal–Organic Complex Arrays", *Inorg. Chem.*, vol. 51, pp. 6437-6439, 2012.

TOWARD CONSTRUCTION OF A VIABLE ARTIFICIAL LEAF FOR SOLAR H2 GENERATION

Nguyen Duc Anh, Tran Dinh Phong
Department of Fundamental and Applied Sciences
University of Science and Technology of Hanoi (USTH), Vietnam Academy of Science and Technology
*Email: tran-dinh.phong@usth.edu.vn

Solar water splitting represents an attractive technology to harvest and store the abundant but intermittent solar energy in the form of chemical energy within the H_2 molecules. It can be realized by using an appropriate photoelectrochemical device, called artificial leaf. In the last two decades, several important advances have been achieved in the identification of suitable catalysts, light harvesting materials as well as artificial leaf engineering. Even though, enormous challenges remain that should be addressed in coming years to make this technology applicable for a viable large-scale production of H_2.

In this talk, we first describe the current state-of-the-art of the solar water splitting research. We then discuss on our current progress in development of noble-metal free catalysts [1-4], nanostructured light harvesters [5] as well as the catalyst/ light harvester assemblage for artificial leaf construction [6].

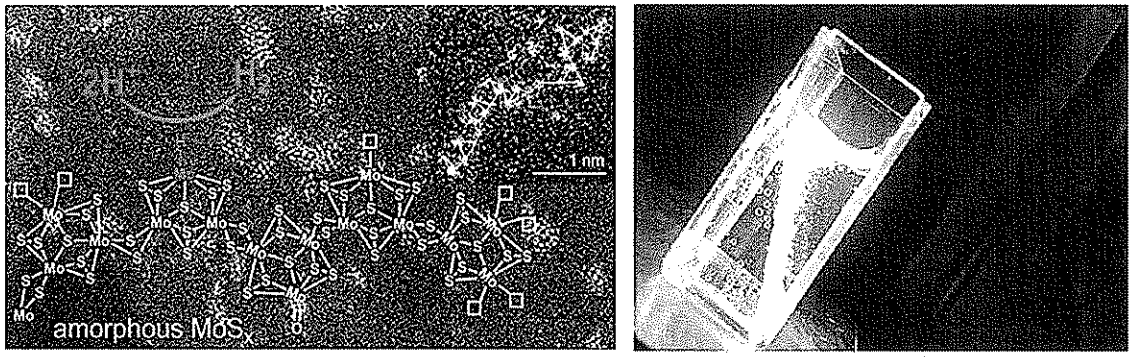

References

1. Phong D. Tran et al, ***Nature Materials***, **2016**, 15, 640-646
2. Quyen T. Nguyen et al, ***ACS Applied Materials Interfaces***, **2018**, 10, 8659-8665
3. Tien D. Tran et al, ***Chemical Communications***, **2018**, 54, 3363-3366
4. Linh N. Nguyen et al, ***Chemistry - An Asian Journal***, **2018**, 13, 1530-1534
5. Hoang V. Le et al, ***International Journal of Hydrogen Energy***, **2018**, 43, 21209-21218
6. Duc N. Nguyen, *unpublished data*

UNVEILING THE NANOPARTICLE-SEEDED CATALYTIC NUCLEATION KINETICS OF PEROVSKITE SOLAR CELLS BY TIME-RESOLVED GIXS

*Chung-Yao Lin,[1,#] **Shao-Sian Li,**[2,3,#] Hao-Chung Chia,[1] Yu-Yun Hsiao,[4] Je-Wei Chang,[5] Chun-Jen Su,[5] Di-Yan Wang,[6] An-Chung Su,[1] Chun-Wei Chen[4,7,8*] & U-Ser Jeng[1,5,*]*

[1]Department of Chemical Engineering, National Tsing Hua University, Hsinchu 30013, Taiwan
[2]Graduate Institute of Biomedical Optomechatronics, Taipei, Medical University, Taiwan
[3] Department of Materials and Mineral Resources Engineering, National Taipei University of Technology (Taipei Tech)
[4]Department of Materials Science and Engineering, National Taiwan University, Taipei 10617, Taiwan.
[5]National Synchrotron Radiation Research Center, Hsinchu Science Park, Hsinchu 30076, Taiwan
[6]Department of Chemistry, Tunghai University, Taichung 40704, Taiwan
[7]Center of Atomic Initiative for New Materials (AI-MAT), National Taiwan University, Taipei 10617, Taiwan
[8]International Graduate Program of Molecular Science and Technology, National Taiwan University (NTU-MST), Taipei 10617, Taiwan

Recently, a new seeding growth approach for perovskite thin films was reported to significantly enhance the device performance of perovskite solar cells. This work unveils the intermediate structures and the corresponding growth kinetics during conversion to perovskite crystal thin films assisted by seeded PbS-nanocrystals (NCs) using time-resolved grazing incidence X-ray scattering (GIXS). Through analyses of time-resolved crystal formation kinetics obtained from the synchrotron X-rays with a fast sub-second probing time resolution, an important "*catalytic*" role of the seed-like PbS nanocrystals was clearly elucidated. The MAI-capped PbS NCs were found to accelerate the nucleation of a highly oriented intermediate phase, and subsequently caused the conversion of the intermediate phase into perovskite crystals with a reaction barrier lower than that when PbS NCs are absent. An activation energy E_a of 47±5 kJ/mol was obtained for the 1 wt% PbS NC-seeded perovskite thin film, compared to 145±38 kJ/mol for the pristine perovskite thin film without the inclusion of PbS NCs. Through the crystal growth kinetics of the perovskite crystal thin films, the underlying mechanisms for enhanced perovskite crystallinity, crystal orientation, and thermal stability of the perovskite thin films seeded with MAI-capped PbS NCs were elucidated, which also explains the significantly improved photovoltaic performance of the corresponding devices.

KEYWORDS: Organo-lead trihalide perovskite, PbS nanocrystals, heterogeneous interface, catalytic additive, grazing-incidence X-ray scattering

TOC GRAPHICS

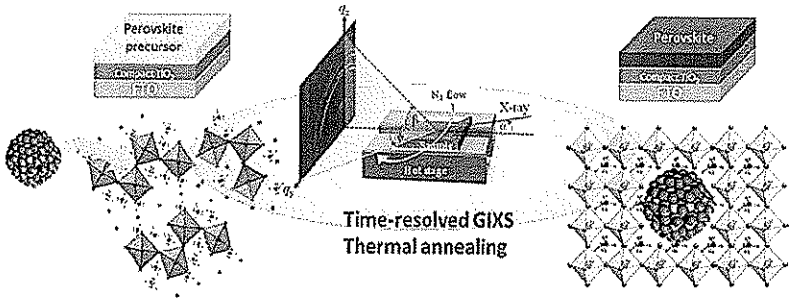

NANOROD CRYPTOMELANE: WATER ADSORPTION STRENGTH AND IMPACT OF METAL DOPING

Tuyet-Mai Tran-Thuy[1,*], Linh-Đang Nguyen[1], Trung Dang-Bao[1], Dung Van Nguyen[1], Hoa-Hung Lam[1], Vo Ke Thanh Ngo[2], Shawn D. Lin[3]

[1]Department of Chemical Engineering, HCMC University of Technology, VNU-HCM, 268 Ly Thuong Kiet, District 10, Ho Chi Minh City, Viet Nam; [2]The research laboratories of Saigon Hi-Tech Park, Ho Chi Minh City, Viet Nam; [3]Department of Chemical Engineering, National Taiwan University of Science and Technology, Taipei 106, Taiwan

*Email: tuyetmai@hcmut.edu.vn

In this work, nanorod OMS-2 (cryptomelane) prepared by sol-gel (OMS-2S), refluxed (OMS-2R) methods and M-OMS-2R (M = Ni and Cr) synthesized by co-precipitation are analyzed by SEM and TEM. Water adsorption over these materials is evaluated by both Langmuir chemisorption and BET physisorption modes. OMS-2S shows the highest water chemisorption strength. In general, the metal doping causes a noticeably decrease of H_2O adsorption strength. The selective oxidation of vapor phase benzyl alcohol with O_2 exhibits a decrease of benzaldehyde yield with the increase of water adsorption strength.

Key words: nanorod cryptomelane, OMS-2, water chemisorption, water physisorption.

INTRODUCTION

The hydrophobicity of cryptomelane – type manganese oxide of octahedral molecular sieves (OMSs) [1], whose structure is shown in Figure 1, was reported to play an important role in catalyzed partial oxidation [2] and decomposition [3] of organic compounds. The hydrophobic index of cryptomelane was typically defined by the molar ratio of benzene uptake and water uptake [3]. However, only few reports discussed how water adsorption strength may influence catalyst performance [4].

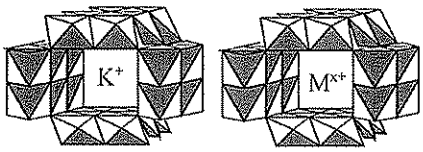

Figure 1: OMS-2 structure with K^+ in the tunnel and M-OMS-2 with M^{x+} cation was substituted for K^+.

Here, we study water adsorption behavior of differently prepared OMS-2 and examine the possible correlation between H_2O adsorption strength and catalyst performance in vapor phase partial oxidation of benzyl alcohol to benzaldehyde.

RESULTS

Sol-gel and reflux methods were applied to synthesize OMS-2S and OMS-2R, respectively. M-OMS-2R (M = Ni, Cr) was prepared by co-precipitation from a mixture of Mn^{7+} and Mn^{2+} according to the previous reports [2, 5]. The size and morphology of OMS-2-based materials were analyzed by SEM and TEM images (Figure 2). Nanorod with a diameter of 5 – 20 nm and a length of 50 – 100 nm were observed for both OMS-2S and OMS-2R, with OMS-2R having a higher aspect ratio. M-OMS-2R had a similar uniform nanorod morphology as that of OMS-2R.

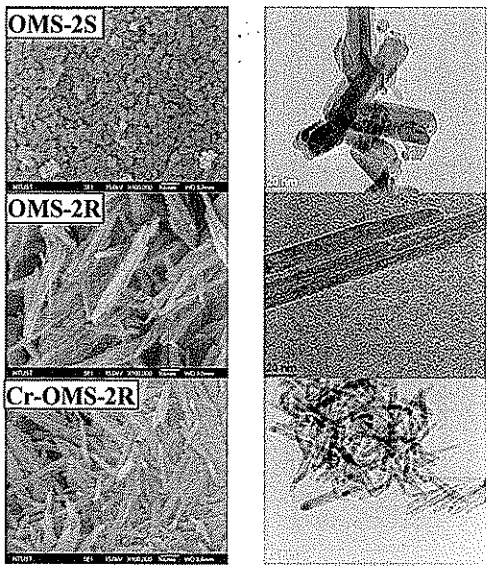

Figure 2: SEM (left) and TEM (right) images of OMS-2S, OMS-2R and Cr-OMS-2.

Water chemisorption (irreversible adsorption) on different OMS-2 materials plotted according to Langmuir adsorption isotherm is illustrated in Figure 3. The linear trend (dash line) observed for OMS-2S, OMS-2R, Ni-OMS-2R samples indicates their consistencies with Langmuir model of both molecular (nondissociative) and dissociative chemisorption.

Conversely, the water adsorption on Cr-OMS-2 did not obey a single stage Langmuir model. As detailed in Table 1, water chemisorption strength (K_{H2O}) on OMS-2S was found higher than that on OMS-2R. The doping of Ni and Cr caused a significant decrease of K_{H2O}. Water physisorption (reversible adsorption) was modeled with BET equation. The H_2O physisorption coefficient (C_{H2O}) of Cr-OMS-2R was found the lowest one indicating a hydrophobic surface caused by metal doping. Yield of benzaldehyde is reported in Table 1. OMS-2R shows a higher yield than OMS-2S and metal doped (Ni-, Cr-) OMS-2R enhanced the benzaldehyde yield. Cr-OMS-2R showed the highest benzaldehyde yield whereas OMS-2S gave the lowest value. Water adsorption analysis reveals water chemisorption strength was the highest on OMS-2S but that on Cr-OMS-2R could not be confirmed (Table 1). In addition, H_2O physisorption parameter from Cr-OMS-2R was the lowest among these OMS-2 materials. This suggests that low affinity of water may play a role in enhancing the catalytic partial oxidation activity of benzyl alcohol over cryptomelane materials.

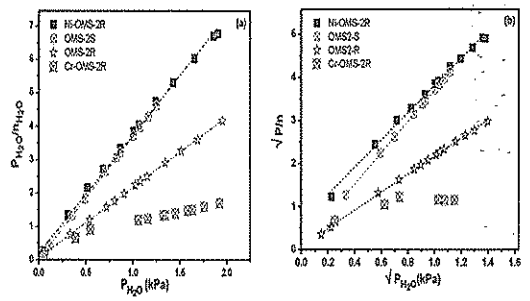

Figure 3: Chemisorbed water obeys Langmuir model of nondissociative (a) and dissociative (b) equations. Water adsorption isotherms was tested following our previous report [6].

Table 1: Water adsorption analysis and yield of benzaldehyde over OMS-2S and M-OMS-2R

Sample	K_{H2O} (kPa^{-1})	C_{H2O}	Yield* of C_6H_5CHO ($mmol/g_{catal}.h$)	Ref.
OMS-2S	147 ± 15	66	8.1	This work
OMS-2R	39 + 2	118	34.2	
Ni-OMS-2R	19 ± 2	80	44.6	
Cr-OMS-2R	-	14	52.5	
Au/TiO_2	-	-	19.6	[7]
OMS-2	-	-	28	[2]

K_{H2O}: H_2O adsorption constant, from fitting of Langmuir nondissociative model.
C_{H2O}: H_2O physisorption coefficient, from fitting of BET model.
(*) Catalyst activity was tested at 280 ^{0}C, a feeding fluid of space velocity of 34.6 $mol_{Alcohol}/hr.g_{catal.}$. Only benzyl alcohol reactant and benzaldehyde existed in liquid product and only CO_2 was collected from gas product.

CONCLUSION

Cryptomelane material synthesized by sol-gel method shows higher water chemisorption strength than one prepared by refluxed method. Metal doping on OMS-2R impacts strongly on water chemisorption strength. High chemisorbed water strength may preclude OMS-2 catalyst activity in selective vapor phase oxidation of benzyl alcohol to benzaldehyde.

ACKNOWLEDGEMENTS

This research is funded by Ho Chi Minh City University of Technology – VNU-HCM under grant number T-KTHH-2018-101.

REFERENCES

[1] Y.-G. Yin, W.-Q. Xu, R. DeGuzman, S.L. Suib, C. O'Young, Studies of stability and reactivity of synthetic cryptomelane-like manganese oxide octahedral molecular sieves, Inorganic Chemistry, 33 (1994) 4384-4389.
[2] N.N. Opembe, C. Guild, C. King'ondu, N.C. Nelson, I.I. Slowing, S.L. Suib, Vapor-phase oxidation of benzyl alcohol using manganese oxide octahedral molecular sieves (OMS-2), Industrial & Engineering Chemistry Research, 53 (2014) 19044-19051.
[3] J. Luo, Q. Zhang, A. Huang, S.L. Suib, Total oxidation of volatile organic compounds with hydrophobic cryptomelane-type octahedral molecular sieves, Microporous and Mesoporous Materials, 35 (2000) 209-217.
[4] T.-M. Tran-Thuy, C.-C. Chen, S.D. Lin, Spectroscopic studies of how moisture enhances CO oxidation over Au/BN at ambient temperature, ACS Catalysis, 7 (2017) 4304-4312.
[5] S. Ching, J.L. Roark, N. Duan, S.L. Suib, Sol– Gel route to the tunneled manganese oxide cryptomelane, Chemistry of Materials, 9 (1997) 750-754.
[6] T.-M. Tran-Thuy, Influences of MOISTURE on ROOM TEMPERATURE CO OXIDATION over Au/BN catalysts, PhD. thesis, NTUST, 2017.
[7] A. Kumar, V.P. Kumar, B.P. Kumar, V. Vishwanathan, K.V. Chary, Vapor phase oxidation of benzyl alcohol over gold nanoparticles supported on mesoporous TiO_2, Catalysis letters, 144 (2014) 1450-1459.

THE ENHANCEMENT OF VISIBLE ABSORPTION OF ZnO NANORODS ON PATTERNED SUBTRATES

Thi My Hoa Tong[1], Van Cat Ha Nguyen,[1] Thi Ngoc Huyen Lai,[1] Cong Khanh Tran,[1] Bach Thang Phan,[2] Vinh Quang Dang[1,2,*]

1 Department of Materials of Science and Technology, University of Science, 227 Nguyen Van Cu street, Ward 4, District 5, Ho Chi Minh City, 700000, Viet Nam.

2 Center for Innovative Materials and Architectures, VNU-HCM, Quarter 6, Linh Trung Ward, Thu Duc District, Ho Chi Minh City, 700000, Viet Nam.

*Email: vinhquangntmk@gmail.com

Abstract

We report the antireflection and light absorption in visible region by new stretchable substrates with patterned structure. Mogul substrates with 3-Dimentional structures were fabricated by using polydimethyl – siloxane that imitate the nanostructures surface. Then, Copper (Cu) doped ZnO nanorods (NRs) on mogul-patterned surface by hydrothermal method at low temperature. The optical properties, morphology and structures of ZnO:Cu NRs were investigated through out of measurement the scanning electron microscopy (SEM), X-Ray diffraction (XRD) and ultraviolet-visible spectroscopy (UV-Vis), respectively. The results show the Cu doped ZnO NRs were uniformly and dense grown on mogul substrates, well oriented in the (002) plane. Additionally, the light absorption can be significantly enhanced to more 10% in a wide spectral range (400-800 nm) due to the reduce reflection. The optical band gap for undoped ZnO (3.13 eV) decreases with Cu concentration-doped ZnO (3.07 eV) is 3%. Growing ZnO NRs on new stretchable substrates with a mogul-patterned surface were successfully fabricated and applicable in the flexible and stretchable optoelectronic devices.

Key words: doping, patterned surface, mogul, ZnO NRs, visible absorption

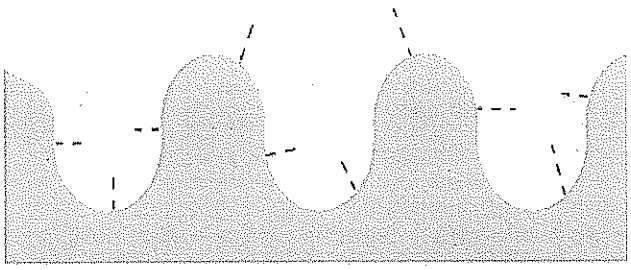

FABRICATION CARBON NANOTUBE ATOMIC FORCE MICROSCOPE PROBE – APPLICATIONS TO SURFACE SCIENCE IN SEMICONDUCTORS AND SCANNING PROBE LITHOGRAPHY

Danh Cong Nguyen, Duong Thai, Tham Nguyen Thi Hong, Thanh Ngo Vo Ke, and Doanh Tu Tieu*
The Research Laboratories of Saigon High Tech Park, District 9, Ho Chi Minh city, Vietnam
*Email: doanh.tieutu@shtplabs.org

Carbon nanotubes are considered to be an ideal imaging probe for atomic force microscopy (AFM) technique because of their small diameter, high strength and high aspect ratio (length to width). In this work, we report the growth CNTs onto Cartridge wire using the Chemical Vapor Deposition (CVD) method and the attachment of individual CNT to Si AFM Probe using a micromanipulator combined with an electric field. The CNT AFM probe can be obtained with CNT length 0.5 - 2 um, diameter 10 – 30 nm and angle between CNT and normal of the cantilever axis $\pm 5^{0}$. Even we can fabricate the apex of CNT with diameter under 5 nm. We also use them to characterize the gold coated on mica surface and fabricate the nanopattern on the Si wafer using the Scanning Probe Lithography technique.

Key words: Carbon nanotubes, Atomic Force Microscope Probe, Scanning Probe Lithography, Chemical Vapor Deposition

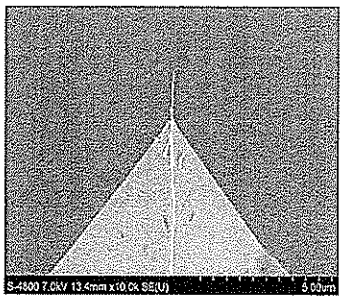

Figure 1. CNT AFM Probe

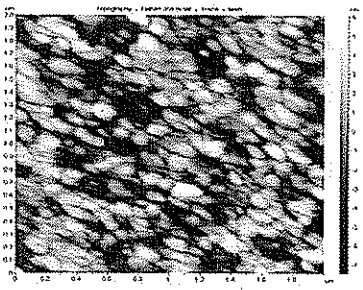

Figure 2. AFM image of Gold coated on mica

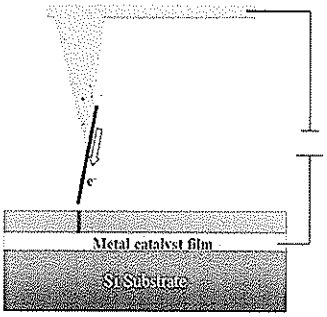

Figure 3. Scanning Probe Lithography Technique

HETERO/HOMOJUNCTION FORMATIONS OF TITANIUM NANOTUBE BY SEVERAL ROUTES WITH ENHANCED PHOTOCATALYTIC ACTIVITY

Vo Cao Minh[1], Phan Tan Dat[1], Nguyen Xuan Sang[2,*]
[1]Department of Environmental Sciences, Saigon University, Ho Chi Minh City, Vietnam
[2]Department of Electronics and Telecommunication, Saigon University, Ho Chi Minh City, Vietnam;
*Email: sangnguyen@sgu.edu.vn

In this study, we successfully fabricated titanium dioxide nanotube (TNT) by a facile hydrothermal method. The synthesized TNT material was annealed at 400°C in the air. Besides, and the composite material between TNT and electrochemical graphene (GrEC) was fabricated similar to the process of TNT which named as T-TNT and TNT@GrEC, respectively. Transmission electron microscope (TEM) images indicated the successful fabrication of TNT with length of several hundred nanometers. In the thermal treatment material, T-TNT, there appeared in both nanotube and nanoparticle types while the composite material (TNT@GrEC) showed the TNT grew on GrEC sheets. Therefore, our result indicated that the formations of homojunction in T-TNT and heterojunction in TNT@GrEC. In addition, the photocatalytic ability for degradation methylene blue (MB) was carried out under direct sunlight irradiation. The photocatalytic efficiencies of T-TNT and TNT@GrEC were better than TNT.

Key words: titanium dioxide nanotube, hydrothermal, annealing, homojunction, photoluminescence.

INTRODUCTION

TiO_2 nanotube (TNT) has been attracted a great attention from scientists worldwide recently due to its fantastic morphological properties with a large specific area and stability for photocatalytic activity [1-3]. However, TNT has a large bandgap, it means that the visible light photocatalytics could not be applied. Many studies have been carried out to reduce the value of bandgap in order to enhance photocatalytic ability [4,5]. The crystal growth mechanism of hydrothermal TNT was studied systematically from temperature induced growing process to hydrochloric acid washing effect on the tube formation [6, 7]. However the thermal stability of synthesized TNT sample and phase transformation of this small nanotube to creating self-homojunction interaction, which has not been received enough attention. Besides, graphene with superior features is one of the leading candidates for improving photocatalytic ability of TNT by formation the heterojunction which induces charge separation. In this study, self-homojunction and heterojunction of TNT were fabricated by a simple thermal treatment and in-situ graphene compositing, respectively. The junction was assigned to the enhanced photocatalytic activity of the materials

RESULTS

Figure 1 shows TEM images of TNT T-TNT and TNT@GrEC. The TNT image indicated the successful fabrication which the tube has homogeneous diameter size ~8 nm and the length of several hundred nanometers. In the annealed sample, T-TNT, there appears both nanotubes and nanoparticles. The particles in T-TNT are quite uniform with the size of 10-12 nm, larger than the tube diameter. TEM image of the composite sample showed the appearance of large graphene sheet covering TNT. The *in situ* hydrothermal growth of TNT in the graphene solution has a longer length than that of pure TNT.

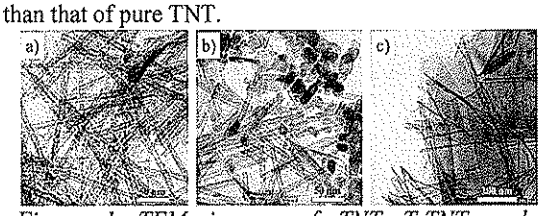

Figure 1 TEM images of TNT T-TNT and TNT@GrEC.

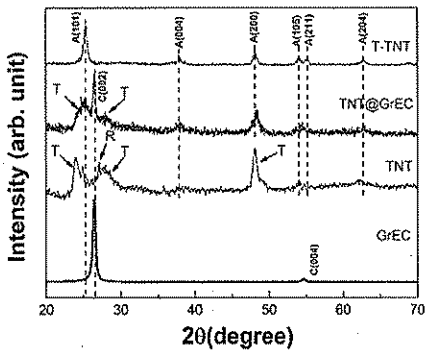

Figure 2 showed XRD patterns of GrEC, TNT and TNT@GrEC composite.

Figure 2 showed XRD patterns of electrochemical graphene (GrEC), TNT and TNT@GrEC composite. XRD characteristic peaks of GrEC locate at 26.42° and 54.71° which are assigned to (002) and (004) directions of graphitic carbon, respectively. The XRD pattern of TNT showed three characteristic peaks at 23.87°, 28.15°, 47.98° corresponding to faces of (110), (211), and (020). Hydrothermally grown TNT in the graphene solution turned the crystal structure of TNT into anatase phase with characteristic peaks at 25.36°, 37.94°, 48.37° and 54.53° corresponding to faces to (101), (112), (200) and (211), respectively. The synthesis of hydrothermal TNT converted from the anatase phase of TiO_2 which changed the phase and structure of the original. XRD patterns of synthesized TNT appear at (2θ) 24.02°, 27.98° and 48.13°.

Figure 1 shows the photocatalytic activity with MB degradation under sunlight irradiation. At the end of the photocatalytic process, the performance of TNT, T-TNT and TNT@GrEC were 41%, 63% and 55%, respectively.

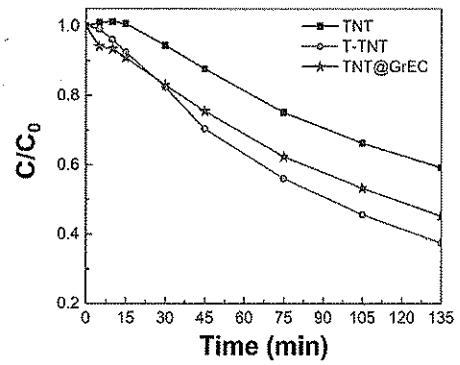

Figure 3 The photocatalytic activity with MB degradation under sunlight irradiation.

CONCLUSION

In conclusion, we successfully created self-homojunction of titanium dioxide nanotubes by thermal treatment and heterojunction of TNT@GrEC composite by insitu grew TNT in graphene solution. The TEM images indicated that the presence of both nanotubes and nanoparticles in the annealed sample (T-TNT); and TNT grew on GrEC sheet in TNT/GrEC. The XRD pattern results determined that the T-TNT has not only in nanotube structure but also anatase phase. The photocatalytic ability is improved for composite and heat-treated samples.

REFERENCES

[1] Qian, L., Du, Z. L., Yang, S. Y. & Jin, Z. S. "Raman study of titania nanotube by soft chemical process". *J. Mol. Struct.* 749, 2005, pp.103–107.

[2] Wong, C. L., Tan, Y. N. & Mohamed, A. R. "A review on the formation of titania nanotube photocatalysts by hydrothermal treatment". *J. Environ. Manage.* 92, 2011, pp. 1669–1680.

[3] F. Jiang, S. Zheng, L. An, and H. Chen, "Effect of calcination temperature on the adsorption and photocatalytic activity of hydrothermally synthesized TiO_2 nanotubes," *Applied Surface Science*, vol. 258, no. 18, 2012, pp. 7188–7194.

[4] S. X. Nguyen, T. Thanh Tung, P. T. Lan Huong, N. H. Tho, and D. Losic, "Heterojunction of graphene and titanium dioxide nanotube composites for enhancing photocatalytic activity," *J. Phys. D. Appl. Phys.*, vol. 51, 2018, no. 26.

[5] N. X. Sang, P. T. L. Huong, T. T. M. Thy, P. T. Dat, V. C. Minh, and N. H. Tho, "Crystalline deformation and photoluminescence of titanium dioxide nanotubes during in situ hybridization with graphene: An example of the heterogeneous photocatalyst," *Superlattices Microstruct.*, vol. 121, 2018, pp. 9–15.

[6] Du, G. H., Chen, Q., Che, R. C., Yuan, Z. Y. & Peng, L. M. Preparation and structure analysis of titanium oxide nanotubes. *Appl. Phys. Lett.* 79, 2001, pp. 3702–3704.

[7] Ou, H. H. & Lo, S. L. Review of titania nanotubes synthesized via the hydrothermal treatment: Fabrication, modification, and application. *Sep. Purif. Technol.* 58, 2007, pp. 179–191.